USDRIVE

DRIVING RESEARCH AND INNOVATION FOR
VEHICLE EFFICIENCY AND ENERGY SUSTAINABILITY

U.S. DRIVE Highlights of Technical Accomplishments 2019

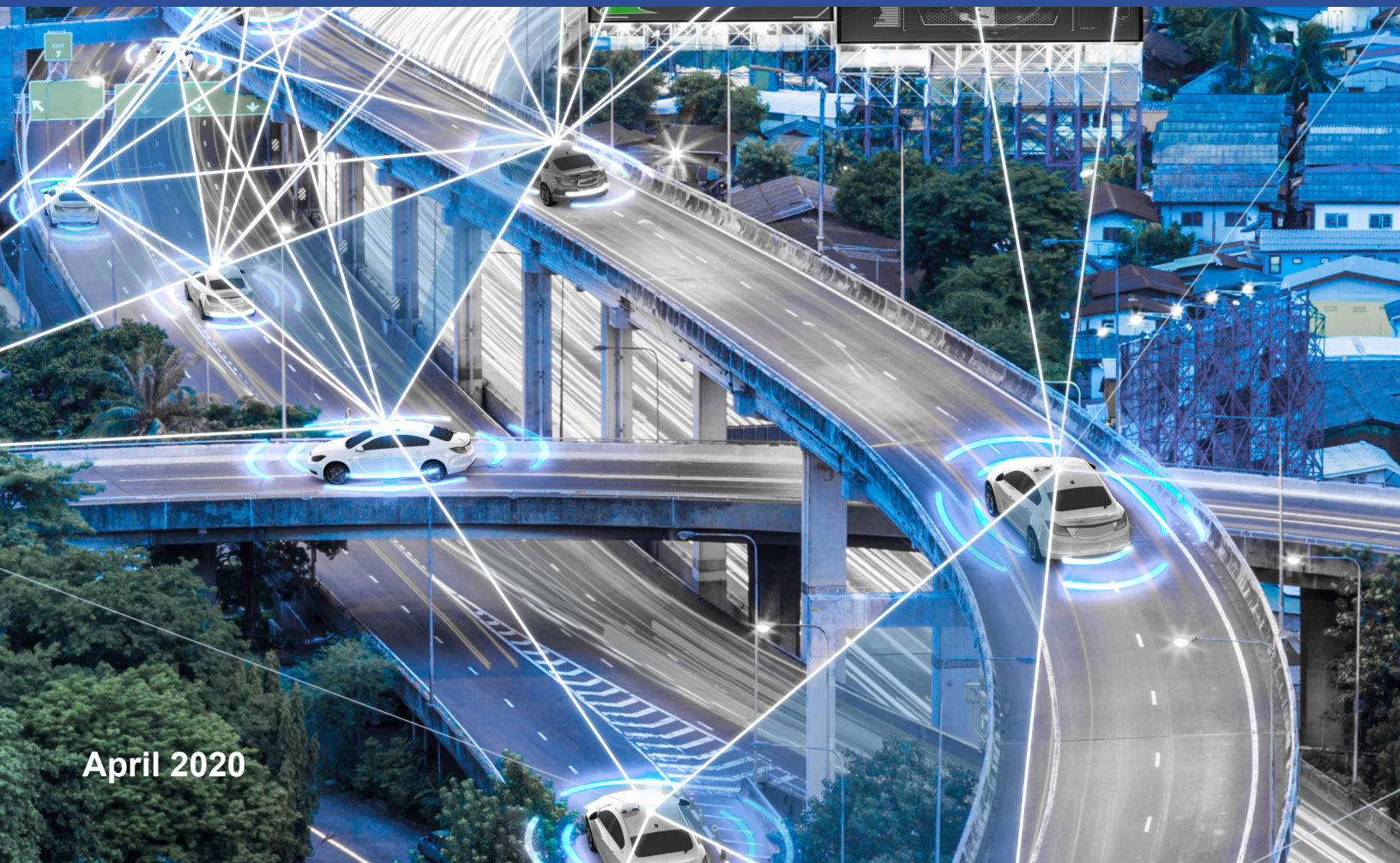

April 2020

U.S. DRIVE
Highlights of Technical Accomplishments Overview

Through precompetitive collaboration and technical exchange, U.S. DRIVE accelerates the development of energy efficient advanced automotive and energy infrastructure technologies.

U.S. DRIVE (*Driving Research for Vehicle efficiency and Energy sustainability*) is a voluntary government-industry partnership focused on precompetitive, advanced automotive and related infrastructure technology research and development. Partners are the United States Department of Energy (DOE) and leaders in the automotive industry (United States Council for Automotive Research LLC, the collaborative technology company of FCA US LLC, Ford Motor Company, and General Motors); energy industry (BP, Chevron, Phillips 66, ExxonMobil, and Shell); and electric utility industry (American Electric Power, DTE Energy, Duke Energy, Southern California Edison, and the Electric Power Research Institute).

The Partnership benefits from a history of successful collaboration across multiple technical areas, each focused on a key area of the U.S. DRIVE portfolio (see below). These teams convene the best and brightest scientists and engineers from across the Partnership to discuss key technical challenges, identify possible solutions, and evaluate progress toward goals and targets published in technology roadmaps. By providing a framework for frequent and regular interaction among technical experts in common areas of expertise, U.S. DRIVE accelerates technical progress, helps to avoid duplication of efforts, ensures that publicly-funded research delivers high-value results, and overcomes high-risk barriers to technology commercialization.

U.S. DRIVE teams selected the highlights in this document from many hundreds of DOE-funded projects conducted by some of the nation's top research organizations. Each one-page summary represents what Partnership experts collectively consider to be significant progress in the development of advanced automotive and infrastructure technologies. The report features technical highlights in two general categories:

Vehicles

- Advanced Combustion and Emission Control
- Electrical and Electronics
- Electrochemical Energy Storage
- Fuel Cells
- Hydrogen Storage
- Materials

Infrastructure and Integration

- Fuels
- Grid Interaction
- Hydrogen Codes and Standards
- Hydrogen Delivery
- Hydrogen Production
- Integrated Systems Analysis

More information about U.S. DRIVE, including prior-year accomplishments reports and technology roadmaps, is available on the DOE (https://www.energy.gov/eere/vehicles/us-drive) and USCAR (www.uscar.org) web sites.

Contents

VEHICLES 1

Advanced Combustion and Emission Control 1

Machine Learning-Based Tools Reduce Combustion Chamber Optimization Cycle from Months to Days 2
Chemical Kinetic Model for Diesel: A Step Towards Higher Fidelity Simulations for Heavy-Duty Engine Design 3
Faster Flame Solvers Enable Higher Fidelity Engine Simulations 4
Insight on Blending Ethanol with Gasoline Improves Prediction of Particle Emissions 5
Catalytic Fuel Reforming Reduces Fuel Consumption by up to 10% 6
Combining Advanced Oxidation Catalyst with Zeolite Trap Significantly Improves Low-Temperature Performance 7
High-Octane Ethanol-Gasoline Blends Reduce Well-to-Wheels Greenhouse Gas Emissions by up to 13% 8
New Catalyst Improves High-Temperature Durability and Efficiency 9
Higher Octane Gasolines Support High-Efficiency, Lean-Burn Spark Ignition Engine Operation 10
New 3D Mapping Diagnostic Provides Insights into Gasoline Spray Dynamics at Realistic Conditions 11
Physics Affecting Injection Variability Discovered 12

Electrical and Electronics 13

Non-Rare-Earth Permanent Magnet Motor with Power Density Reaching the 5.7 kW/L Target 14
Higher Temperatures of Power-Dense Electric Machines Improve Fluid Jet Impingement Cooling Performance 15
Nanocarbon-Enabled Ultra-Conducting Copper Composites with Improved Electrical Conductivity 16
Low-Loss Iron Nitride Composite Magnets 17

Electrochemical Energy Storage 18

EverBatt: Model Predicts Battery Lifecycle Cost and Environmental Impacts with Key New Findings 19
New Electrolytes Eliminate Shuttle Effect, Towards Higher Cycle Life Lithium-Sulfur Cells 20
Stabilizing Silicon Anodes via Simple New Electrolyte Additives Towards Higher Energy Density 21
High-Performance Lithium-Metal Cell Technology 22
Improved Performance in High-Nickel Cathodes via Surface Conditioning Synthesis Protocols 23
Cathode Cracking Phenomena in Fast-Charging Newly Identified as a Focus Area for Durability Improvement 24
Effect of Binder Morphology and Crystal Structure on Electrode Performance 25
Freeze Casting Innovation for Composite Cathode Architectures in All Solid-State Lithium Batteries 26
Surface Dopants to Stabilize High-Nickel Cathodes 27
Zero-Strain Layered-Rocksalt Intergrown Cathodes for Future High-Energy Density Cell Development 28
Cobalt-Free Cathode Synthesis, Scale-up, and Performance 29
Cathode Electrode Structuring with CoEx Printing Improves Performance of Thick Electrodes 30
Maximizing Fast Charging of Lithium-Ion Batteries via Real-Time Detection of Lithium Plating 31

Fuel Cells 32

Performance and Durability Models Highlight Path to Reaching DOE Targets 33
Platinum-Gold Alloy Cathode Catalyst Achieves 3x Stability 34
Characterization of a Fuel Cell Electrode Transport 35
Improved High-Power Performance of Fuel Cell Catalyst 36

Hydrogen Storage Technical Team 37

Leveraging Cooperative Materials Development Efforts to Reduce the Cost of Hydrogen and Natural Gas Storage 38
Cost of a 700 bar Type IV Hydrogen Storage System Significantly Reduced 39

Materials *40*
Graphene-Based Solid Lubricants for Automotive Applications 41
Development and Integration of Predictive Models for Manufacturing and Structural Performance of Carbon Fiber Composites in Automotive Applications 42
Thin Advanced High-Strength Steel with Carbon Fiber Reinforced Polymer Coatings 43
Machine Learning and Supercomputing to Predict Corrosion/Oxidation of High-Performance Valve Alloys 44
Higher Conductivity Copper Yields Higher Efficiency Electric Motors 45
Room-Temperature Stamping of High-Strength Aluminum Alloys 46
Corrosion Control in Carbon Fiber Reinforced Plastic Composite-Aluminum Closure Panel Hem Joints 47
A Multi-Scale Computational Platform for Predictive Modeling of Corrosion in Aluminum-Steel Joints 48
Low-Cost Magnesium Sheet Component Development and Demonstration Project 49

INFRASTRUCTURE AND INTEGRATION 50

Grid Interaction *50*
Unified Model Tying Electric Vehicles with Other Grid Energy Resources Now Available for Researchers 51
Electric Vehicle Market Projections: Scenarios and Impacts 52
The Energy Management Circuit Breaker, Phase 2 53

Hydrogen Codes and Standards *54*
Development of an In-Line Hydrogen Contaminant Detector 55

Hydrogen Delivery *56*
Hydrogen Refueling Station Footprint Analysis 57

Hydrogen Production *58*
New PGM-Free Catalysts and Membranes Improve Performance of Alkaline Membrane Electrolyzers 59
Path to $2/kg Hydrogen from Polymer Electrolyte Membrane Electrolysis Identified 60

Integrated Systems Analysis *61*
Past Growth in U.S. Electric Load Exceeds Additional Consumption and Peak Demand in Future EV Scenarios 62
Automated Vehicle Lightweighting and Smooth Driving Offset Automation Load for a Net Reduction in Greenhouse Gas Emissions in Base Case 2030 Scenario 63

VEHICLES

Advanced Combustion and Emission Control

2019 U.S. DRIVE Highlight

Machine Learning-Based Tools Reduce Combustion Chamber Optimization Cycle from Months to Days

Optimization technique combining machine learning and computational simulations shows that it can significantly shrink industrial design cycles for developing advanced automotive engines.

Argonne National Laboratory

The traditional approach to co-designing a piston bowl with an injection strategy for engines involves multiple iterations of experimental prototyping and testing. More recently, high-fidelity computational simulations together with high performance computing have assumed a much greater significance in engine design optimization. However, traditional virtual optimization approaches combining algorithms, such as design of experiments (DoE) and genetic algorithms (GA) remain time consuming, due to long simulation runtimes.

Researchers at Argonne National Laboratory (ANL) developed a novel optimization technique, known as Machine Learning – Genetic Algorithm (ML-GA), which leverages machine learning to speed up virtual engine design. In this approach, rigorously validated computational fluid dynamics (CFD) simulations are employed to generate the requisite engine data from which machine learning (ML)-based surrogate models are developed to predict engine performance as a function of the design parameters. These faster surrogate models are coupled with GA to rapidly optimize the engine design parameters, in terms of maximizing efficiency while satisfying constraints associated with emissions, engine mechanical limits, etc. The surrogate model development methodology utilizes the advanced "Superlearner" technique, which uses multiple ML algorithms (such as Random Forest, Neural Networks, etc.) to obtain better predictive accuracy than any of the constituent learning algorithms alone. In addition, an efficient active learning strategy is used to minimize the simulation data required for training the surrogate model. ANL researchers demonstrated the novel ML-GA approach for engine design, considering various parameters related to piston bowl geometry, fuel injection, etc. ML-GA reduced time-to-design by 80% (from a few months to a few days) compared to traditional methods. This demonstration was done in collaboration with Aramco researchers on ANL's Mira supercomputer.

ANL researchers, in collaboration with industry partners *Parallel Works* and *Convergent Science*, have now implemented their copyrighted ML-GA software technology in an end-to-end ML workflow. The new workflow, developed under U.S. Department of Energy's Technology Commercialization Fund, can be leveraged by the piston engine community.

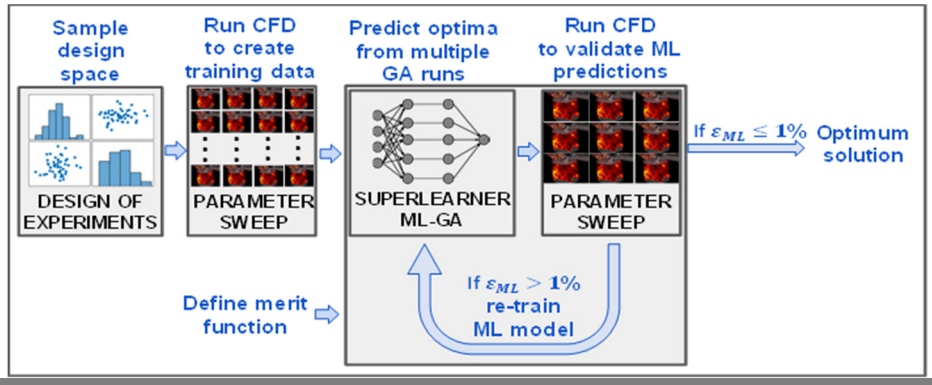

Figure 1. A schematic of the ML GA workflow for design optimization.

2019 U.S. DRIVE Highlight

Chemical Kinetic Model for Diesel: A Step Towards Higher Fidelity Simulations for Heavy-Duty Engine Design

The kinetic model has fuel components that allow the matching of chemical functional groups, ignition properties, distillation curve, and density of a target diesel fuel.

Lawrence Livermore National Laboratory

Researchers have developed a detailed chemical kinetic model with surrogate molecules representative of the different chemical classes in diesel fuel. The surrogate molecules have chemical functional groups and boiling points representative of those found in real diesel fuels and their inclusion enables high-fidelity simulation of diesel fuel ignition. Researchers validated the surrogate kinetic model for single and multicomponent fuels by comparing simulated results with experimental results from rapid compression machines (RCM), shock tubes, and jet stirred and flow reactors (Figure 1). The detailed chemical kinetic model for diesel fuel can be used to simulate fuel effects in internal combustion engines.

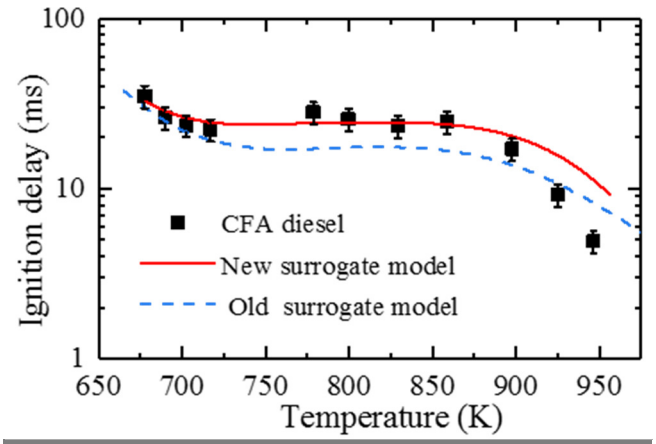

Figure 1. Comparison of simulated (lines) and measured (symbols) ignition behavior in an RCM for a diesel certification fuel. Simulations use a new diesel surrogate kinetic model with an 8 component surrogate mixture and an old surrogate model with a 2 component surrogate mixture (diesel primary reference fuel). Experiments: Kukkadapu, C. J. Sung, Combust. Flame 166 (2016) 45 54.

The detailed diesel surrogate model has been reduced in size (number of species and reactions) so that it can be used in multidimensional simulations of a reacting diesel spray. The multidimensional simulations using the reduced model captures the effects of ambient oxygen concentration on ignition delays and flame lift-off lengths (Figure 2). In summary, a high-fidelity chemical kinetic model for diesel fuel has been developed, reduced in size, and can be used in engine simulation codes to provide more accurate predictions of combustion phasing, heat release, and species concentrations.

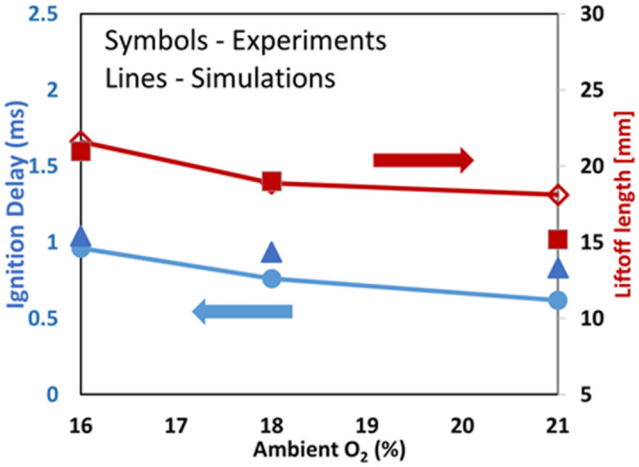

Figure 2. Comparison of experimental and simulated ignition delays and flame lift off lengths from spray ignition of a diesel certification fuel in a constant pressure chamber at engine conditions. Simulations were conducted using a tabulated flamelet model, a reduced version of the Lawrence Livermore National Laboratory diesel surrogate model with 1544 species and a 4 component surrogate from the Coordinating Research Council. Experimental data are from M. Kweon, J. Temme and V. Coburn at US Army Research Laboratory. Simulations were conducted at Argonne National Laboratory by P. Kundu, C. Xu, and S. Som.

2019 U.S. DRIVE Highlight

Faster Flame Solvers Enable Higher Fidelity Engine Simulations

Flame solvers use an approximation of the chemical system to greatly reduce the cost associated with matrix operations resulting in speedup of up to 100 times compared to current state of the art.

Lawrence Livermore National Laboratory

Researchers have developed laminar flame solvers that are up to 100 times faster than currently available commercial codes. The new solvers enable the inclusion of higher fidelity chemical kinetics important for capturing knock and emissions in engine simulations and demonstrate a path for reducing the computational cost of species transport in computational fluid dynamics (CFD) simulations.

Laminar flame solvers are used to calculate the speed at which an un-stretched laminar flame propagates through a mixture of reactants. These calculations are used in a wide array of applications, such as validation of chemical mechanisms and generation of lookup tables for engine CFD combustion models. Currently available flame solvers are inefficient in dealing with the large chemical mechanisms used for transportation fuels. Typically, these mechanisms will need to be reduced prior to table generation, reducing model fidelity and requiring engineering expertise and time.

Researchers at Lawrence Livermore National Laboratory (LLNL) developed unsteady and steady solution methods for both premixed and diffusion laminar flames. The flame solver reduces the cost of matrix operations by using intelligent approximations of the chemical system, without reducing accuracy. The flame solvers were validated through comparisons against the Chemkin commercial code and were found to be in excellent agreement (Figure 1). For a large (2800 species) gasoline mechanism, LLNL's solvers are 100 times faster than commonly-used commercial codes (Figure 2). These solvers have been used to generate flame speed lookup tables for CFD simulations of boosted spark-ignition engines (collaboration with Argonne National Laboratory) and to compute the sooting tendencies of different transportation fuels (collaboration with Penn State University and Yale University).

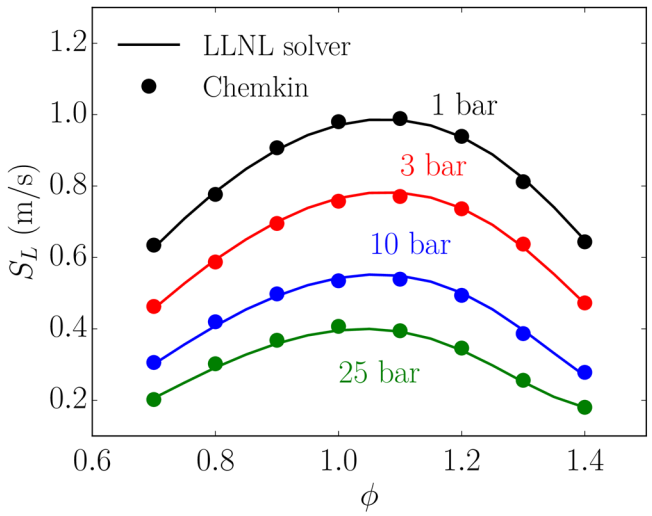

Figure 1. Laminar flame speeds of n heptane/air flames at different pressures and equivalence ratios. Results obtained with the LLNL solver compare well with those obtained using the commercial code Chemkin.

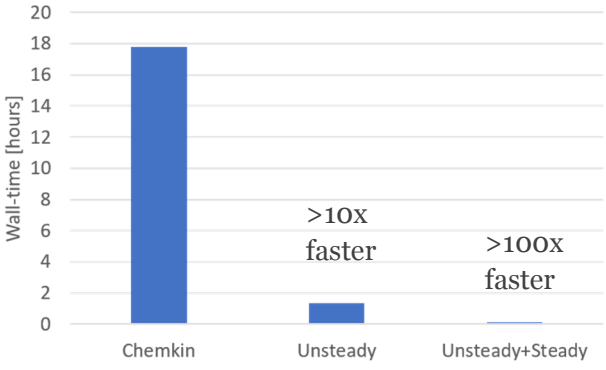

Figure 2. Wall clock times for a sweep of eight equivalence ratios with the 2878 species Co Optima gasoline mechanism. Timing results from the commercial code Chemkin and the LLNL unsteady and steady solvers are compared (reduced wall clock times indicate faster simulations).

2019 U.S. DRIVE Highlight

Insight on Blending Ethanol with Gasoline Improves Prediction of Particle Emissions

Improved model includes interactive ethanol aromatic evaporation terms and yield sooting index, dramatically improving the ability to predict particulate matter.

National Renewable Energy Laboratory

The National Renewable Energy Laboratory developed an improved model for predicting particulate matter (PM) emissions from gasoline properties. It includes interactive terms for ethanol and aromatic content, as well as aromatic yield sooting index and vapor pressure. Because aromatics are the primary source of PM emissions from spark ignition engines, dilution of aromatics by blending ethanol into gasoline is expected to reduce PM. A reduction of PM is also predicted for ethanol blends by the current state-of-the-art particulate matter index (PMI) model. However, literature reports that ethanol blending increases PM emissions in some cases, while reducing it in others. Gasoline direct injection (GDI) engines are particularly sensitive to fuel property effects on PM, because fuel spray impinging onto cylinder walls and pistons inhibits fuel evaporation, leading to combustion in rich zones and/or pool fires. Thus, better models to predict PM from fuel properties can facilitate control of PM emissions from GDI engines over the range of ethanol-gasoline compositions allowed in the market.

Researchers used a designed fuel matrix to investigate ethanol's contradictory effects on PM reported in the literature. New analytical chemistry techniques and single-droplet fuel evaporation modeling showed that ethanol affects hydrocarbon vapor-liquid equilibria, which inhibits aromatics' evaporation and concentrates aromatics within the shrinking fuel droplets. This effect coupled with ethanol's increased evaporative cooling leads to longer fuel droplet lifetimes and aromatic enrichment within the evaporating droplets. These effects compete with ethanol's dilution of the aromatics. Consequently, when combusting fuels containing a low vapor pressure aromatic (t-butyltoluene) in a GDI engine at high speed and load, ethanol blending significantly increased PM emissions, revealing ethanol's inhibitory effects on aromatics/droplet evaporation. However, at the same operating conditions PM emissions were insensitive to ethanol blending for fuels containing a higher vapor pressure aromatic (cumene), demonstrating that ethanol's dilution and inhibitory effects were balanced. The linear regression model developed from this study predicted these PM emission results from fuel properties, with an R^2 value of 0.97 (see Figure 1), compared with 0.69 from the PMI model. Reducing fuel spray impingement by splitting fuel into two equal injections significantly reduced PM emissions from all fuels. Moreover, ethanol effects that increased PM from the low vapor pressure aromatic fuels were attenuated, such that blends with and without ethanol produced the same PM emissions, within measurement error.

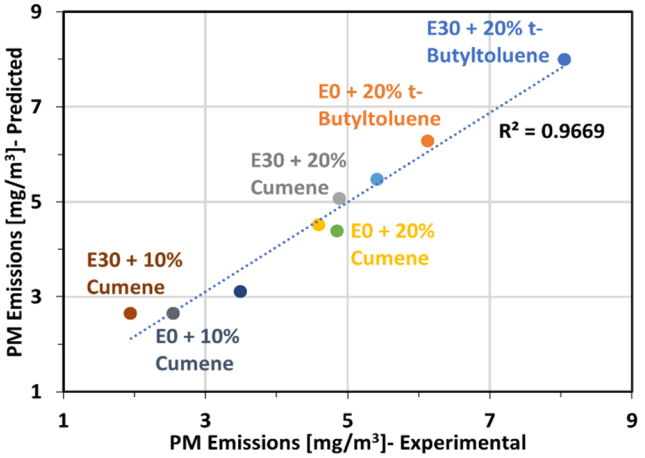

Figure 1. Improved PM model provides strong correlation by linear regression. Figure adapted from Impact of Ethanol Blending into Gasoline on Aromatic Compound Evaporation and Particle Emissions from a Gasoline Direct Injection Engine. Ratcliff, et al., *Applied Energy*, Vol. 250, **2019**, 1618 1631, https://doi.org/10.1016/j.apenergy.2019.05.030.

2019 U.S. DRIVE Highlight

Catalytic Fuel Reforming Reduces Fuel Consumption by up to 10%

Dilution limit extension and recovery of exhaust waste heat saves fuel across a wide engine load range while maintaining compatibility with conventional emissions controls.

Oak Ridge National Laboratory

Researchers at Oak Ridge National Laboratory (ORNL) implemented a combustion strategy that included extending the dilution limit with cooled exhaust gas recirculation (EGR) combined with recovery of waste heat in the exhaust, both of which are known methods of improving engine efficiency. EGR dilution limit extension was achieved by reforming a portion of the fuel in the EGR-loop to generate a reformate mixture high in hydrogen. Waste heat recovery was also achieved by reforming through thermochemical recuperation (TCR), where a portion of the waste heat in the exhaust was converted to chemical energy in the reformate. Additionally, to ensure emissions compliance, this method was implemented in a way that maintains compatibility with a conventional three-way catalyst by maintaining stoichiometric exhaust.

The reforming strategy utilized a rhodium-based catalyst formulation that had been previously developed by Delphi and Umicore. Synthetic exhaust flow reactor studies of the catalyst at ORNL allowed for regions of efficient reforming, including TCR, to be identified. These boundary conditions, which required low concentrations of oxygen (less than 2 vol%) in a fuel-rich environment (Φ greater than 5), were then reproduced on the engine by isolating one of the cylinders to feed the catalyst so that it could be operated differently than the other cylinders. Despite composition differences between cylinders, engine load was balanced across all 4 cylinders with acceptable stability (coefficient of variation in indicated mean effective pressure of less than 3%).

The presence of the reformate allowed extension of the EGR dilution limit from less than 25% to greater than 36%. Further, the researchers showed that the peak temperature in the reforming catalyst could be controlled by setting the reforming catalyst boundary conditions, even as the engine load was increased, thereby mitigating concerns about catalyst durability. The resulting strategy improved brake engine efficiency over a wide range of loads as shown in Figure 1, including boosted operation. This engine operation strategy reduced fuel consumption by up to 10% relative to baseline operation without EGR. The efficiency improvements were accompanied by a decrease in exhaust temperature of nearly 100°C, though the resulting exhaust temperatures are still sufficiently high to maintain three-way catalyst functionality.

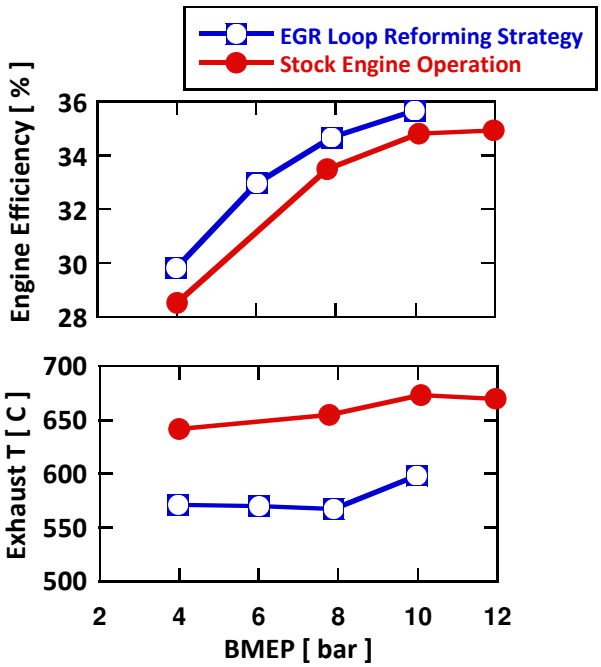

Figure 1. Engine efficiency and exhaust temperature for the EGR loop reforming strategy compared to the stock engine operation, illustrating an efficiency increase across a wide operating range while maintaining stoichiometric exhaust for compatibility with conventional emission controls.

2019 U.S. DRIVE Highlight

Combining Advanced Oxidation Catalyst with Zeolite Trap Significantly Improves Low-Temperature Performance

Combining an Oak Ridge National Laboratory designed oxidation catalyst and a zeolite based trap achieved 90% conversion for hydrocarbons in full simulated exhaust mixtures after moderate aging.

Oak Ridge National Laboratory

Oak Ridge National Laboratory (ORNL) is developing low-temperature and durable emissions control solutions to address key hurdles limiting introduction of advanced combustion technologies and high-efficiency powertrains. Higher efficiency engines have lower exhaust temperatures, and electrified powertrains can generate multiple cold start/re-start events during normal driving. When combined with increasingly stringent emissions standards, which may incorporate real-world emissions regulations, high-efficiency vehicles face significant emissions control challenges. To address these challenges, ORNL is developing catalyst components (known as supports) that enhance the activity of precious metal catalysts at low temperatures while also maintaining this activity after exposure to high-temperature aging and sulfur poisoning. These supports provide a high surface area that allows the catalysts to interact with the gases in the exhaust. The goal is to achieve 90% conversion of criteria pollutants at 150°C using the U.S. DRIVE protocols, which are found at https://cleers.org/low-temperature-protocols/.

ORNL has developed an advanced silica@zirconia (core@shell) support for precious metals. This unique structure offers a stable, high surface area zirconium (Zr) oxide surface to disperse palladium (Pd) and platinum (Pt), which leads to enhanced activity compared to Zr-only. Although the activity achieved with this sample is very good, further improvements are necessary to reach the goal of 90% conversion at 150°C. When this Pt+Pd/silicon dixodie@Zr dioxide oxidation catalyst (Pd+Pt/S@Z) is combined with a material that can trap both hydrocarbons and nitric oxide, ion-exchanged Pd/zeolite (Pd/ZSM-5), the reactivity is significantly enhanced even after moderate aging at 800°C for 10 h. Although the SiO_2@ZrO_2 support offers significant stability, aging it for 50 h and exposing it to sulfation/desulfation cycles leads to further deactivation; however, combining the oxidation catalyst with a zeolite trap shows a promising pathway to meeting the 150°C challenge.

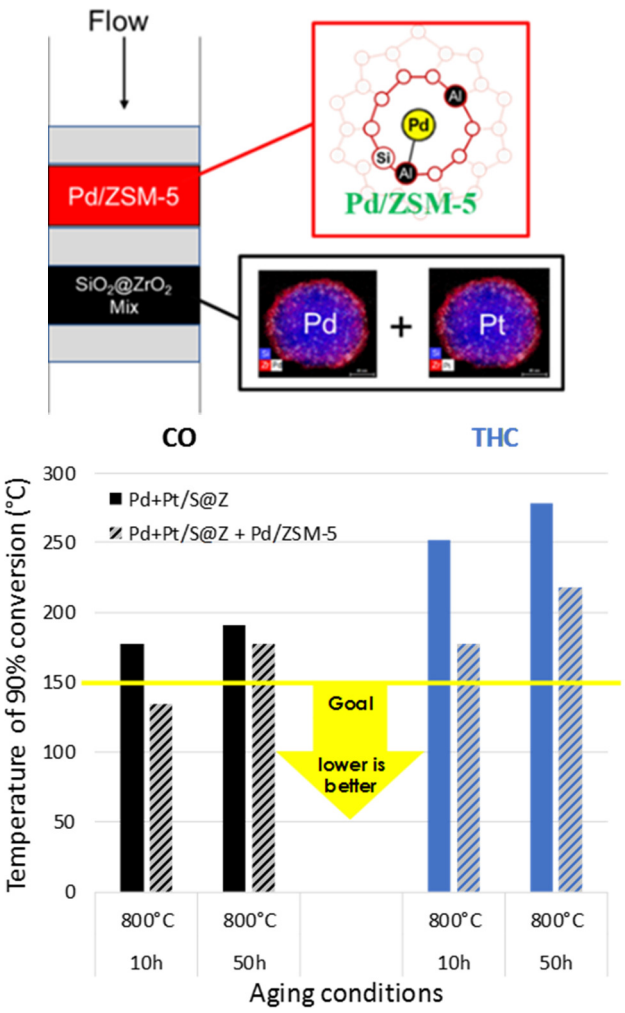

Figure 1. Combining an ORNL developed advanced oxidation catalyst/support, Pt+Pd/SiO_2@ZrO_2, with a trapping material, Pd/ZSM 5, significant improvements in low temperature reactivity were achieved that show a pathway towards 90% conversion at 150 C under U.S. DRIVE evaluation conditions.

2019 U.S. DRIVE Highlight

High-Octane Ethanol-Gasoline Blends Reduce Well-to-Wheels Greenhouse Gas Emissions by up to 13%

U.S. DRIVE Fuels Working Group study quantifies benefits of both higher engine efficiencies enabled through higher octane fuels, and increased biofuel content.

Oak Ridge National Laboratory, Argonne National Laboratory, and the U.S. DRIVE Fuels Working Group

U.S. DRIVE formed the Fuels Working Group (FWG) to study fuel effects on combustion. The FWG evaluated several fuel and engine combinations to determine if there are more optimal fuel/engine combinations that could be designed and deployed in the future. In the broadest perspective, the research compares various high-octane number fuels in the context of engine performance and their relative life-cycle carbon impacts, as well as potential impacts on fueling infrastructure and associated costs.

The study focused on high-octane gasolines that contained biofuel blendstocks including ethanol (up to 30%), bioreformate surrogate, and a wood-based biogasoline. The candidate fuels were studied in a Ford EcoBoost 1.6-liter engine at Oak Ridge National Laboratory (ORNL) to provide engine data for a well-to-wheels (WTW) greenhouse gas (GHG) study conducted by Argonne National Laboratory. The GHG study incorporated refinery models to determine manufacturing energy use and GHG emissions for each fuel blend.

The results demonstrated that increased compression ratio enabled by raising the research octane number (RON) of gasoline can lead to reductions in both WTW GHG emissions and in energy use by the light-duty vehicle fleet. Blending biofuels to achieve the RON increase can provide even greater GHG benefits, with ethanol demonstrating up to 13% reduction (with E30) compared to baseline for a 97-RON fuel. Greater benefits can be attained using 101-RON fuels (Figure 1).

Although GHG emissions reductions are driven primarily by biofuel blend level in the fuel, the improvement in engine efficiency is also important. It is not always possible to increase both engine efficiency and fuel economy simultaneously when using biofuels because these fuels often have a lower energy content than gasoline. The engine efficiency increase enabled with 97 RON fuel was high enough to offset the reduced energy content of the E20 fuel, providing improved fuel economy in addition to reducing both energy use and GHG emissions in mixed driving styles. Blending 30% ethanol provides even greater reduction in energy use and GHG emissions but causes fuel economy to drop by about 3%–5%.

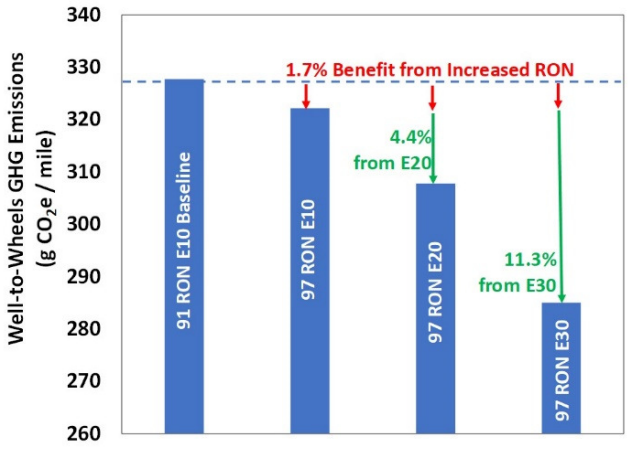

Figure 1. Blending higher quantities of biofuels such as ethanol into gasoline can provide substantial reductions (up to 13%) in WTW GHG emissions; 1.7% of that increase is due to higher engine efficiency enabled by increasing gasoline RON from 91 to 97.

2019 U.S. DRIVE Highlight

New Catalyst Improves High-Temperature Durability and Efficiency

A novel catalyst circumvents a formidable catalyst aging pathway, thus improving catalyst performance and durability compared to current state of the art commercial catalysts.

Pacific Northwest National Laboratory

Improved exhaust aftertreatment performance is necessary to further reduce criteria pollutant emissions and enable widespread deployment of more efficient combustion strategies in transportation. This improvement is needed to span both low and high temperatures and must also be accompanied by retained high-temperature stability. For lean combustion systems, chabazite zeolite ion-exchanged with copper (i.e., Cu-CHA) is currently considered the state-of-the-art for selective catalytic reduction (SCR) of nitrogen oxides (NO_x) owing to its activity and durability. However, under extreme operating conditions, the stability of Cu-CHA can weaken resulting in inferior performance and hastened degradation. Recent research by Pacific Northwest National Laboratory (PNNL) has led to the discovery of a modification to current state-of-the-art Cu-CHA formulations that will improve the durability and extend the high-temperature NO_x reduction efficiency of the catalyst under extreme operating conditions.

In Cu-CHA catalysts, the active component for SCR is Cu ions held in place by the zeolite. However, under extreme conditions, Cu can migrate out of the zeolite to form CuO. This CuO degrades performance by oxidizing ammonia (NH_3) before it can be used for NO_x reduction. This CuO can also damage the zeolite structure thus accelerating the catalyst's degradation.

PNNL researchers have developed a strategy to circumvent the adverse impact of CuO species on Cu-CHA formulations. The strategy involves incorporating a secondary zirconium dioxide (ZrO_2) phase in a highly dispersed fashion to the parent Cu-CHA catalyst.

The resulting ZrO_2-modified Cu-CHA selectively binds CuO in a way that significantly reduces its NH_3 oxidation activity. Additionally, binding the CuO, ZrO_2-modified Cu-CHA prevents CuO from inflicting further damage on the SCR catalyst. This strategy increases the durability of Cu-CHA formulations and improves its high-temperature selectivity by ensuring NH_3 is available for SCR and not oxidized. Furthermore, ZrO_2-modified Cu-CHA formulations enable increased Cu loading into the catalysts for additional SCR functionality without suffering from the typical decrease in durability.

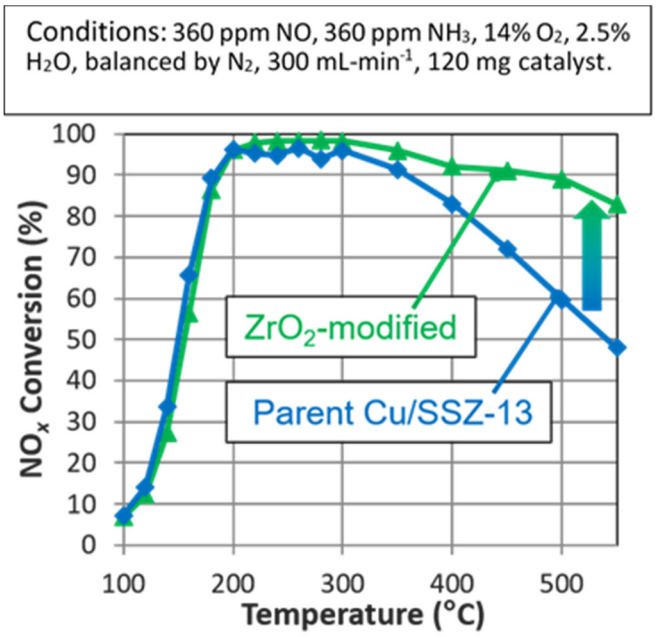

Figure 1. Cu CHA catalyst (i.e., parent Cu SSZ 13) versus ZrO_2 modified Cu SSZ 13, demonstrating superior NH_3 SCR efficiency above 300 C attributed to reduced parasitic NH_3 oxidation from CuO.

2019 U.S. DRIVE Highlight

Higher Octane Gasolines Support High-Efficiency, Lean-Burn Spark Ignition Engine Operation

The octane related fuel requirements that benefit spark ignition engines also benefit advanced combustion that uses a combination of spark ignition and compression ignition.

Sandia National Laboratories

Engine downsizing and turbocharging are widely used to reduce fuel consumption of spark-ignition (SI) engines. However, the higher engine loads and cylinder pressure make the engine operation more limited by abnormal combustion that causes audible knock, restricting the maximum compression ratio (CR) and therefore limiting the engine's efficiency potential. Fuels that have a high octane number and a high octane Sensitivity S (the difference between the Research and Motor octane numbers) are known to increase knock resistance, allowing a higher CR and improved fuel economy.

Another way to reduce the vehicle fuel consumption is to utilize "mixed-mode" lean combustion for moderate loads and speed, where the engine spends most of its time. Here, a spark initiates the initial combustion and as the mixture burns it heats and compresses the unburned mixture, leading to a controlled autoignition that speeds combustion and increases efficiency. This high-efficiency, mixed-mode SI/compression ignition (CI) combustion is also known as SACI (spark assisted compression ignition) combustion. However, it is not obvious that an engine that combines conventional SI combustion at high load and mixed-mode combustion at lower loads has the same fuel requirements as mainstream boosted SI engines.

To resolve this question, researchers used a combination of experiments and modeling to determine the octane requirement of the SI/CI mixed-mode combustion process in the 1,000–2,000 rpm engine speed range typical of automotive drive cycles. The results show that the fuel-requirement synergies between conventional stoichiometric SI and mixed-mode combustion are strong. High octane fuels allow higher loads for mixed-mode combustion, as do high Sensitivity fuels. The higher loads allow lean combustion to be used more frequently during practical driving with widely varying torque demand, reducing fuel consumption. Fuels with high Sensitivity reduce the effect of intake boosting and increased CR on autoignition, further extending both the efficiency and upper mixed-mode load limits, as illustrated in Figure 1.

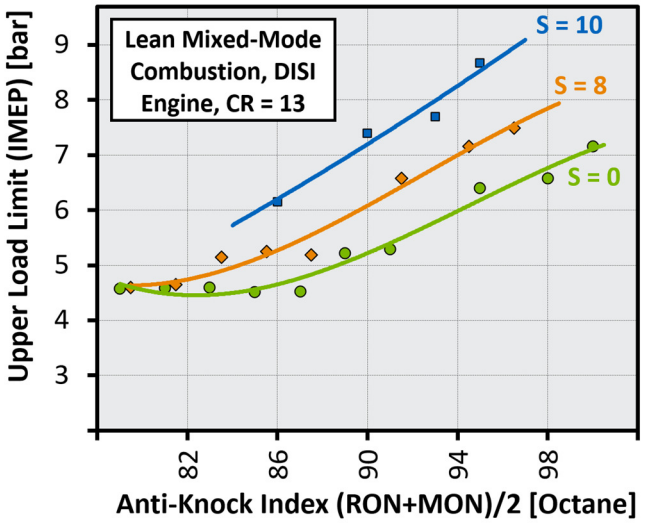

Figure 1. Effect of increasing anti knock index (AKI) and octane sensitivity (S) on the upper load limit of highly efficient lean mixed mode combustion.

In summary, both increasing octane and increasing S act to extend the load-range coverage with lean mixed-mode combustion. High octane and high S fuels thus benefit conventional SI combustion, while concurrently maximizing the benefit that can be derived from mixed-mode combustion at lower loads—ultimately enabling higher efficiencies from both operating modes.

2019 U.S. DRIVE Highlight

New 3D Mapping Diagnostic Provides Insights into Gasoline Spray Dynamics at Realistic Conditions

A new high speed diagnostic for gasoline spray three dimensional liquid distribution provides understanding and computer model validation datasets needed to improve mixture formation.

Sandia National Laboratories

Gasoline direct-injection (GDI) must be executed precisely to control knock and cold-start emissions. Although current multi-hole fuel injectors are designed to widely disperse and mix fuel, interaction between plumes may cause "collapse" into a single jet resulting in poor mixing, over-penetration, and impingement—leading to elevated particulate matter emissions and inefficiency. Understanding how fuel properties affect the fuel delivery is also of critical importance for engine and injector design.

To better characterize spray behavior, researchers at Sandia National Laboratories have developed a new high-speed diagnostic to map the three-dimensional distribution of multiple plumes at representative engine conditions. Extinction imaging is applied to an 8-hole injector at different rotational orientations, followed by computed tomography reconstruction, yielding the geometry and motion of each plume resolved in time after start-of-injection (aSOI). Liquid-volume fraction distributions shown (Figure 1) are the ensemble average of many injections, comparing results for iso-octane (a single-component reference fuel with 99°C boiling point) to E30 (a wide-range distillate fuel containing 30% ethanol). While plumes remain separate for iso-octane, allowing rapid mixing and vaporization, the E30 plumes collapse together creating a poorly mixed core that is slow to vaporize and a repeatable toroidal vortex at the spray head.

The understanding provided by these unique datasets is key for computer model validation activities. The optical techniques and accompanying datasets are also transferrable to industry for the design and optimization of GDI systems tolerant to a wide variety of operating conditions and future renewable fuels.

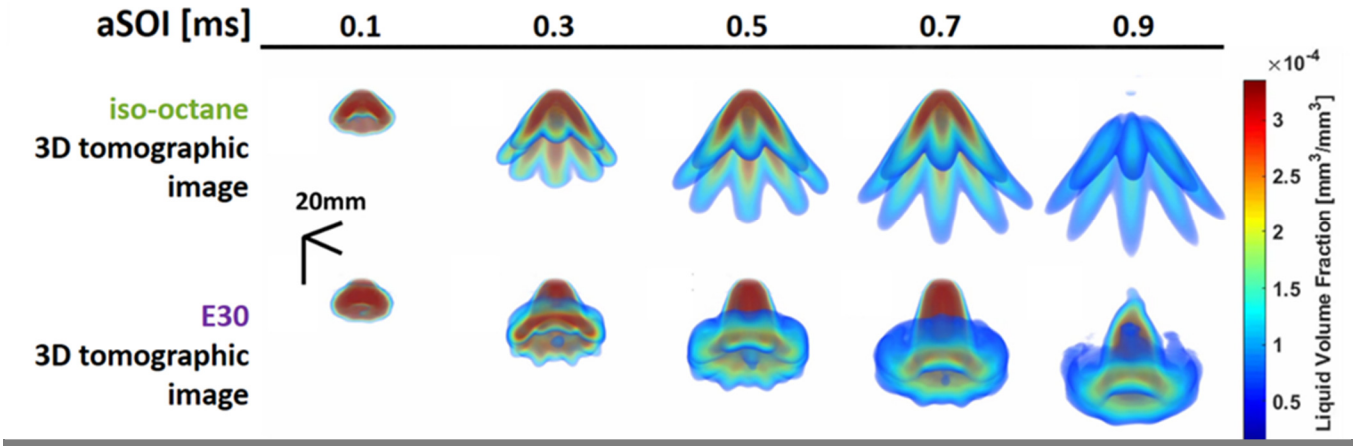

Figure 1. Gasoline spray 3D renderings showing how iso octane fuel (top) is much different than 30% ethanol gasoline (bottom) even with the same injector and conditions. ECN 8 hole Spray G, 90 C, 200 bar, injection duration 0.78 ms. Ambient conditions: 60 C, 0.5 bar.

2019 U.S. DRIVE Highlight

Physics Affecting Injection Variability Discovered

High speed imaging in a transparent nozzle shows that end of injection cavitation begins a chain of events that evacuates significant liquid from the injector and alters the subsequent injection event.

Sandia National Laboratories

Precise control of fuel injection is critical to the development of clean, high-efficiency diesel and gasoline engines. Modern injection systems use multiple injections with many opening and closing events. Understanding and predicting how the injector and spray respond to these transients is essential to improve performance.

Researchers at Sandia National Laboratories manufactured transparent nozzles with the same hole inlet radius and diameter as an actual injector, mounted to a functioning injector body and needle valve at realistic fuel pressures. They applied high-speed microscopic imaging at speeds exceeding 100 kHz to understand flow transients throughout injection. Figure 1 shows dynamics at the end of injection using select frames in a time panel that begins slightly before the end of injection. With backlighting, the sac and nozzle appear clear—indicating transmissive liquid fuel rather than vapor bubbles that block and scatter light. As the needle valve closes and pressure decreases, cavitation vapor bubbles form momentarily within the sac and hole. But as pressure equilibrates, the cavitation zones collapse back to liquid fuel, creating a vacuum that pulls ambient gas into the fuel injector. Further imaging (not shown) reveals that these gas bubbles expand as pressure decreases during an expansion cycle, which can empty the injector sac of liquid fuel. Importantly, the change in the initial state of the injector from liquid to gas dramatically alters delivery of the next injection, including the liquid dispersion and rate of injection (right-hand figure).

This imaging study reveals previously unknown physics affecting transient injection. Computer models are now under development to account for these physics to optimize new injector hardware.

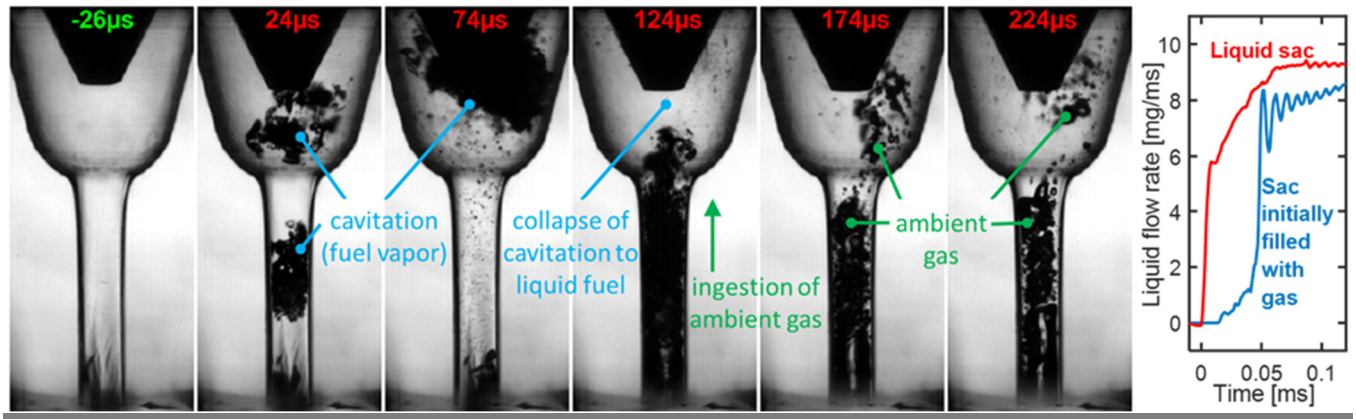

Figure 1. High speed microscopic imaging in a 0.18 mm single hole transparent diesel nozzle during the ending of injection. Time is shown in green before the end of injection and red after needle valve closure. The fuel is n dodecane and the injection pressure is 500 bar. The figure on the right shows how (via simulation) the rate of injection is altered when sac is filled with gas.

Electrical and Electronics

2019 U.S. DRIVE Highlight

Non-Rare-Earth Permanent Magnet Motor with Power Density Reaching the 5.7 kW/L Target

An MnBi permanent magnet prototype is built and tested, meeting design specifications.

Iowa State University, Ames Laboratory, University of Delaware, and United Technology Research Center

A powerful motor requires a powerful permanent magnet (PM). Neodymium (Nd)-iron (Fe)-boron (B) is the most powerful PM developed to date, but Nd is a critical element subject to high supply risk. Non-rare-earth (non-RE) magnets, composed of ferrites, are weak, with a maximum energy product less than 10% of what Nd-Fe-B can offer. Although a motor made with non-RE magnets costs substantially less than a RE-PM motor, the cheaper motor is bulky and inefficient. Nd-Fe-B therefore remains the preferred magnet for electric vehicle (EV) applications. With the exponential growth of the EV market, demand for Nd is expected to grow proportionally, and the supply risk for Nd is expected to escalate.

Iowa State University (ISU) and Ames Laboratory (AMES) are working together to develop a powerful non-RE magnet whose maximum energy product could reach 50% of Nd-Fe-B's strength. The magnet uses manganese (Mn) and bismuth (Bi), neither of which is a critical element. Although weaker than the Nd-Fe-B magnet at 300 K, the non-RE magnet offers better temperature dependence thanks to its ability to gain resistance to demagnetization fields at higher temperature. Researchers found that MnBi's coercivity increases as the temperature rises, whereas Nd-Fe-B's coercivity decreases with increasing temperature. As a result, Mn-Bi's performance nears that of Nd-Fe-B at higher temperatures (above 300 K). The ISU-AMES team has completed composition and process optimizations and fabricated 80 bulk magnets (Figure 1), which are ready for testing in a motor.

In parallel with the ISU-AMES work, the United Technology Research Center (UTRC) team designed a high-power density motor to validate the potential of the novel MnBi magnet. In 2018, UTRC completed the design of a 10 kW 360 Hz motor with 5.7 kW/L power density (a U.S. Department of Energy target). The motor uses 300 model magnets with magnetic properties closely matching MnBi's properties. The prototype was built in 2019 and tested with the standard protocols, meeting design specifications for both efficiency and power density. The prototype was also stress-tested at 400 Hz and delivered 11 kW power with an efficiency over 91%.

The mass-produced MnBi magnets have a nominal maximum energy product of 8 MGOe. An advanced materials team at the University of Delaware has successfully developed a new chemistry and demonstrated a small magnet (0.1 gram) with 12 MGOe. Researchers expect that, with further composition and process optimizations, an MnBi magnet with 15 MGOe could be mass-produced. These vastly improved properties will lead to a much more powerful non-RE motor.

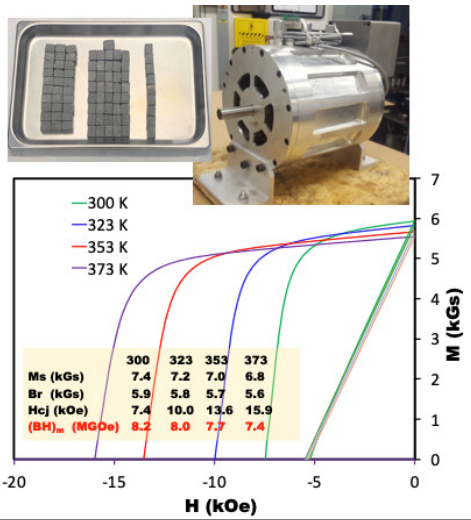

Figure 1. Demagnetization curves of the MnBi magnet at 300 to 373 K. Each bulk magnet is 1 cm^3 and 9 g. The motor is designed to deliver 10 kW at 360 Hz. It was tested at 400 Hz and delivered 11 kW.

2019 U.S. DRIVE Highlight

Higher Temperatures of Power-Dense Electric Machines Improve Fluid Jet Impingement Cooling Performance

Database of automatic transmission fluid jet impingement cooling results shows that increasing the temperature of power dense electric machines could improve heat removal rates.

National Renewable Energy Laboratory

Driveline fluids allow the removal of heat—generated in machine or power electronics components—directly from the point of heat generation. This technique is being considered for electric machine and power electronics cooling applications.

The National Renewable Energy Laboratory (NREL) developed a database of heat transfer coefficients (HTCs) or rates for jet impingement cooling with automatic transmission fluid (ATF). The research team evaluated several parameters: fluid temperature, impingement velocities, cooled surface topography (features emulating wire bundles of different wire gages), surface temperatures, and jet impingement angles/locations. The measurements are applicable for electric machines with wire windings (Figure 1), including high-rpm electric machines under development for future electric vehicles. NREL also plans to characterize jet impingement cooling for bar/hairpin windings, which requires modifying the experimental setup.

Figure 1. Experimental setup for HTC measurements for ATF jet impingement cooling.

Results show HTC enhancements at jet velocities of 2.5–7.5 m/s due to surface wire-bundle features. Recent experimental outcomes indicated that the higher temperatures of the cooled surface results in higher HTC values. Increasing the surface temperature (flat/plain surface) from 90°C to 120°C enhanced HTCs by up to 15% (Figure 2).

This effect is likely due to elevated fluid film temperature near the heated surface, resulting in reduced viscosity (a strongly temperature-dependent property for ATF) above the hot surface. Lower viscosity leads to a thinner viscous boundary layer, thereby increasing fluid flow and reducing the thickness of the thermal boundary layer as well. The HTC rises as a result of higher temperature gradients in the thinner thermal boundary layer.

The database of measured HTCs is helping automotive original equipment manufacturers, electric machine manufacturers, and the broader research and development community with design and development of compact, high-performance, and reliable machines that use driveline fluids for thermal management.

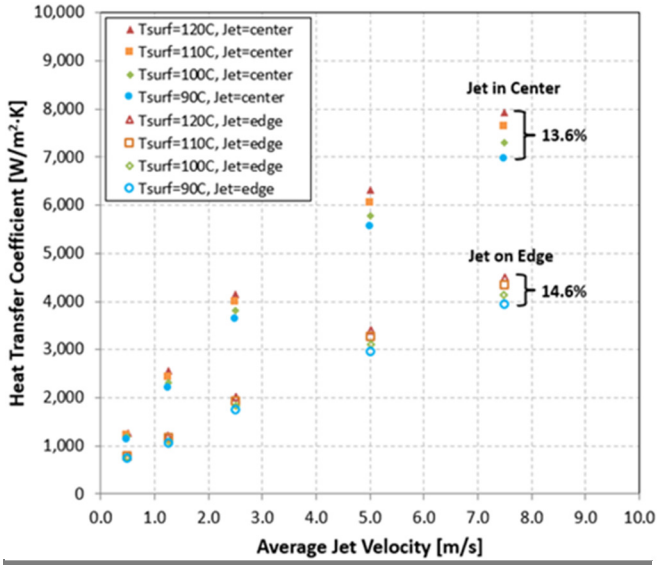

Figure 2. HTC values for ATF jet impingement cooling with 50 C fluid with jet in the center and the edge of the cooled target surface.

2019 U.S. DRIVE Highlight

Nanocarbon-Enabled Ultra-Conducting Copper Composites with Improved Electrical Conductivity

Ultra-conductive copper composites promise higher electric drive power densities and efficiencies.

Oak Ridge National Laboratory

The power losses associated with the electrical resistance of copper (Cu) have adverse impacts on the efficiency and performance of all electric devices. In the case of electric motors, reductions in volume and improvements in efficiency are limited in part by the electrical conductivity limitations of Cu windings. The stator with Cu winding constitutes nearly 40% of the total motor cost, so a key U.S. DRIVE R&D focus is to reduce cost by using new materials with improved capabilities and performance and applying them in motor design innovations.

In ballistic electrical transport, charge carriers can travel over approximately 500 nm in carbon nanotubes (CNTs) without scattering. This approach is expected to improve the Cu matrix's conductivity, with additional CNT-enabled benefits, including low weight, flexibility, and better thermal management. A few promising Cu–CNT composites (UCCs) with improved conductivities have been demonstrated—but only on micrometer-long sample pieces. Further improvements to these UCCs have been hampered by poor fundamental understanding of Cu–CNT interactions, specifically how they affect bulk electrical and thermal transport properties. In addition, most of the present UCC processing strategies are unstable (leading to inconsistent results) and are limited to laboratory-scale operations, rendering these methods unsuitable for large-scale commercial development and production.

Researchers at Oak Ridge National Laboratory (ORNL) have demonstrated a new approach that couples theoretical and experimental efforts to enable the design and scalable, reproducible assembly of Cu–CNT multilayer composites that have electrical conductivity exceeding that of pure Cu. Using a physical property measurement system, researchers measured temperature-dependent electrical properties of single- and multi-layer Cu–CNT–Cu composites at various temperatures ranging from 0°C to 125°C. Results shown in Figure 1 demonstrate that, compared to the reference pure Cu sample, electrical resistivity is reduced more than 5% for one-stack Cu–CNT–Cu and more than 10% for three-stack prototypes over the entire temperature range.

ORNL then analyzed the impact of using such higher-conductivity composite conductors for the winding of traction motors. Researchers found that a UCC composite with 30% higher conductivity than pure Cu can enable a 10% reduction in the active volume for conventional motors and a 12% reduction for motors in which magnetic saturation is not an issue.

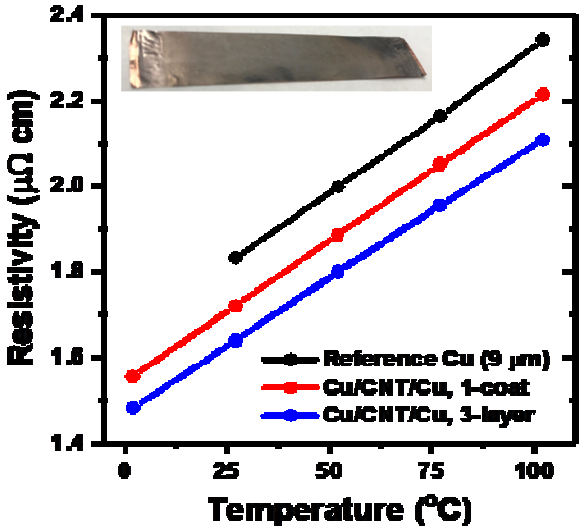

Figure 1. Electrical properties of single- and three-layer Cu–CNT–Cu composite architectures as a function of temperature ranging from 0°C to 120°C, displaying reduced resistivity as compared to the reference Cu substrate. The inset shows a photograph of a-stack Cu–CNT–Cu prototype.

2019 U.S. DRIVE Highlight

Low-Loss Iron Nitride Composite Magnets

Increasing efficiency in both power electronics (inductors) and electrical motors through bottom up soft magnetic composites.

Sandia National Laboratories

Soft magnetic materials are a significant source of loss in both power electronics and electric motors. Improved soft magnets will lead to increased efficiencies in inductors for both electric drives and electrical machines. A new bottom-up approach to soft magnetic composites (SMCs) leveraging a new soft magnetic material, iron nitride (γ'-Fe_4N), is a promising solution.

Researchers at Sandia National Laboratories began their investigations by developing a new method to create phase-pure Fe_4N from mixed-phase, commercially available iron nitride powder. The starting material is a mixture of both Fe_3N and Fe_4N. A straightforward heat treatment converts the Fe_3N phase to the higher-saturation magnetic polarization (J_s = 1.89 T) Fe_4N phase. Temperature-dependent X-ray diffraction (XRD) data for this process, collected under flowing nitrogen, is displayed in Figure 1. These data show that at a temperature slightly above 550°C, the diffraction peaks associated with the F_3N disappear, leaving nearly phase-pure Fe_4N.

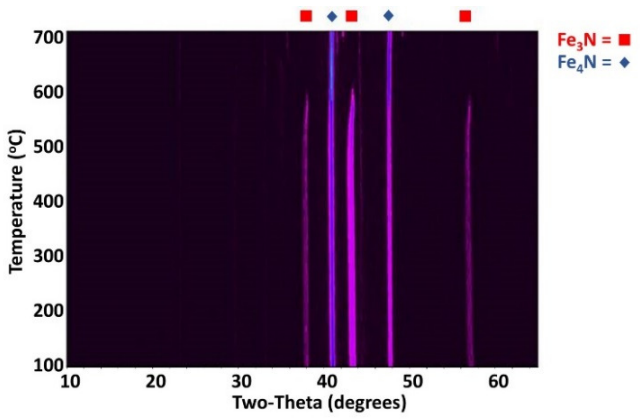

The research team also developed a process to fabricate the iron nitride–epoxy composite cores, using Sandia's own custom epoxy formulations. First, iron nitride powder is milled with diamine molecules until they are well coated, as confirmed by infrared spectroscopy. Next, the amine functionalized magnetic particles are mixed with a di- or tri-epoxide terminated molecule. This mixture is then poured into a three-dimensional (3D)-printed mold and cured, forming a cross-linked epoxy-based composite. An image of three cured magnetic composite cores wound for B-H analysis is shown in Figure 2.

The researchers fully expect that the magnetic properties will be significantly enhanced as the processing conditions and the volume loading of the magnetic particles are optimized. For example, hot pressing will be used to create higher-volume loading magnetic composites, which will be particularly beneficial for increasing the energy density in non-rare-earth electric motors. Furthermore, in the upcoming fiscal year, the Sandia team will develop a process to 3D-print composite inductor cores.

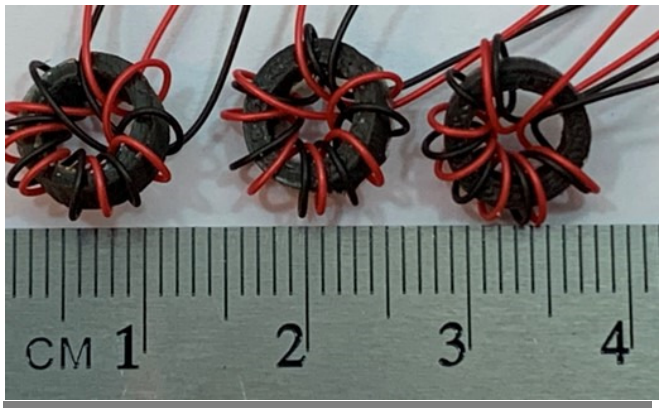

Figure 2. Magnetic composite toroidal inductor cores wound for B H analysis.

Electrochemical Energy Storage

2019 U.S. DRIVE Highlight

EverBatt: Model Predicts Battery Lifecycle Cost and Environmental Impacts with Key New Findings

EverBatt is an easy to use, Excel based model that calculates the costs and environmental impacts at various stages of a battery s life, especially for recycling.

Argonne National Laboratory

EverBatt is a closed loop model used to estimate cost and environmental impacts throughout a product's lifespan, in this case lithium-ion batteries. With the exception of the "Battery Use" stage, Figure 1(a) shows various lifecycle stages of a battery that are included in the model. This free, Excel-based model has been used by industry, academia and government to help identify and evaluate many battery lifecycle questions. Though the tool can be used for any stage of a battery's life, the initial focus of the model has been on recycling. Some examples of how this new type of model can be useful include:

- Identification of the highest impact lifecycle stages of a product's life
- Comparison of processes within a particular lifecycle stage
- Comparison of a virgin battery to a battery manufactured with recycled content.

When comparing the different lifecycle stages of a lithium-ion battery, the model identified that the cost of transportation for recycling could, in some instances, be higher than the cost of recycling itself (Figure 1(b)). This finding helped start the push to search for improved methods of transporting batteries at the end of life to help reduce overall product cost.

Another important finding exemplified in Figure 1(c) is that closed loop recycling via any technology provides a lower overall environmental impact during the battery manufacturing stage than that of using virgin material; however, the cost can be higher. An opportunity was found that direct cathode recycling can dramatically improve the economics and environmental impacts of recycling and thus lower the cost of new batteries.

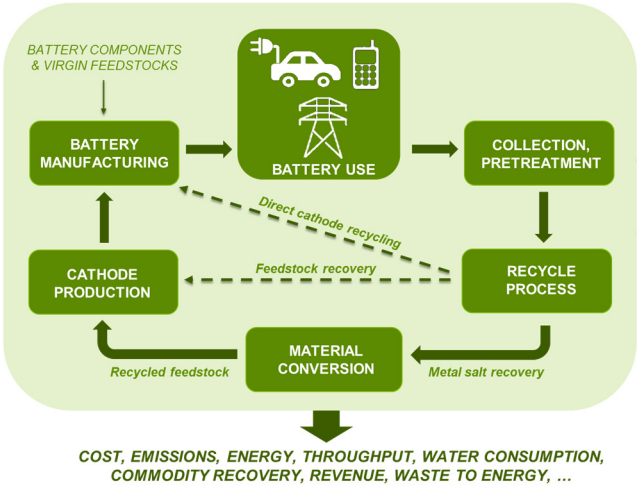

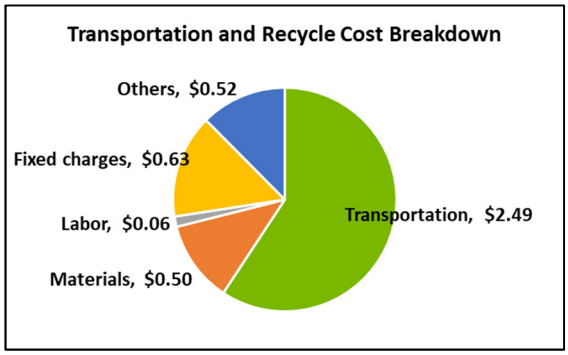

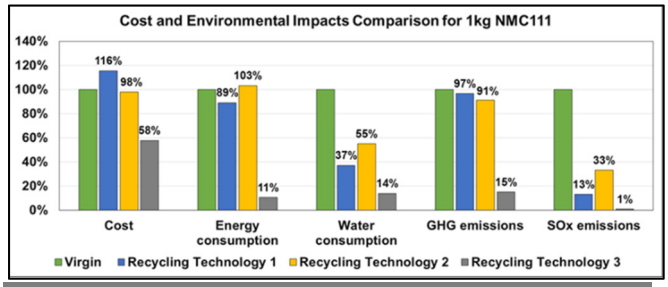

Figure 1. (a) EverBatt s flowsheet, (b) Example breakdown of a lithium ion battery recycling cost, including transportation, and (c) Chart comparing battery manufacturing cost and environmental impacts from virgin material and material provided by generic examples of 1: pyro, 2: hydro, and 3: direct recycling.

2019 U.S. DRIVE Highlight

New Electrolytes Eliminate Shuttle Effect, Towards Higher Cycle Life Lithium-Sulfur Cells

A new fluorinated electrolyte suppresses shuttle effect and improves cycle life. Selenium doping increased the electronic conductivity of sulfur and enabled improved sulfur electrode loading.

Argonne National Laboratory

Lithium/sulfur (Li/S) batteries are very attractive for automotive and grid application because of their high theoretical energy density (2600 Wh/kg) and the global natural abundance of sulfur. However, two major obstacles to their use are the poor electronic conductivity of sulfur and the lithium polysulfide shuttle. Integrating sulfur with various carbon hosts has been the most common approach to improve the performance of Li/S batteries due to the high electronic conductivity and the polysulfides' confinement by many carbon hosts. However, polysulfides have high solubility in conventional ether-based electrolytes, which can be readily detached from the host materials and lead to severe capacity fade and poor coulombic efficiency. In addition, carbon is electrochemically inactive, which reduces the overall energy density.

Researchers at Argonne National Laboratory have developed a new strategy by using fluorinated ether electrolyte (1.0 M LiTFSI/DOL+TTE+0.2M $LiNO_3$) and selenium (Se) doping of sulfur to improve the electrochemical performance of Li/S batteries. The TTE-based electrolyte eliminates the formation of polysulfides (X-ray absorption near edge structure [XANES] data, not shown, found no evidence of polysulfide dissolution after cycling) and enables a solid-solid lithiation process, which is quite different from the two-step solid-liquid-solid lithiation process in conventional DME-based electrolytes (Figure 1a). This has been confirmed by the in-situ Se K-edge X-ray absorption near edge spectroscopy. The result showed that there is no energy shift for Se, only intensity variation of Se (12658 eV) during discharge and charge, as shown in Figure 1b.

Also, we used Se doping to increase the utilization of S due to the comparable volumetric capacity and high electronic conductivity of Se compared to S. The electrochemical test results showed that by using only 10wt.% Se doping, the rate and cycling stability were improved as shown in Figure 2. Although Se is currently too expensive to be used in mass produced automotive cells, researchers believe that this strategy could serve as a promising guide for fast-charging Li/S batteries with high coulombic efficiency and long life.

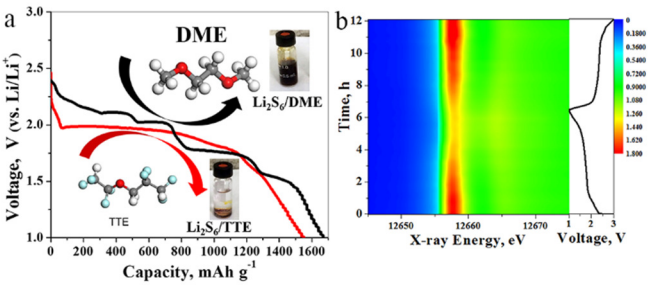

Figure 1. (a) First discharge curve of S_5Se_2/C cathode in DME based electrolyte and TTE based electrolyte; (b) In situ Se K edge XANES spectra of S_5Se_2/C cathode in TTE based electrolytes at C/10.

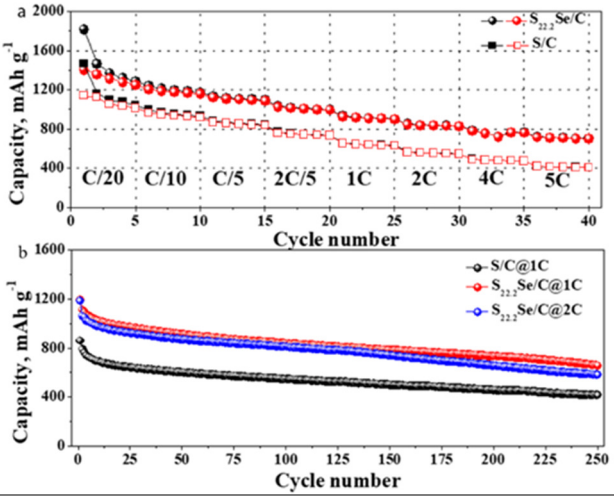

Figure 2. Rate performance and cycling performance at high rates of $S_{22.2}$Se/KB cathode and S/KB cathode in TTE based electrolyte.

2019 U.S. DRIVE Highlight

Stabilizing Silicon Anodes via Simple New Electrolyte Additives Towards Higher Energy Density

Mixed salt electrolytes paired with silicon anodes are shown to promote in situ formation of a stabilizing nanoscale compound that enhances cycle life.

Argonne National Laboratory and National Renewable Energy Laboratory

The rapid development of electric vehicles (EVs) has created a demand for next-generation, higher energy, and lower cost lithium (Li)-ion batteries. While the commercial graphite anode has excellent properties, its inherent maximum capacity has become a fundamental barrier in improving the energy density of cells. Replacing the traditional graphite anode with a pure silicon (Si) anode would theoretically create an electrode with 10 times the gravimetric capacity of graphite. The enhanced capacity is tied to a Li storage mechanism that requires bond breaking within the Si lattice (compared to Li intercalation between graphite sheets which requires no bond breaking), in addition to creating reactive lithiated Si compounds that chemically reduces common binders and electrolyte components. Together, these processes combine to reduce the amount of active Li over cell life, break down free electrolyte solvent, disrupt binder surface interactions, and contaminate interfacial surfaces, resulting in low cycling efficiencies and a relatively poor life (compared to graphite cells).

We successfully reduced the reactivity of the surface while maintaining performance by adding 0.1M $M(TFSI)_x$ (M = Mg, Zn, Al and Ca) salt in addition to standard $LiPF_6$ into the electrolyte, stabilizing the anode through in situ formation of surface Li–M–Si phases during charging. These new electrolytes were tested in commercially relevant but non-optimized single layer pouch cells made by Argonne's Cell Analysis Modeling and Prototyping Facility. Cells tested showed superior cyclability and higher coulombic efficiencies in both half-cell and full-cell configurations (except for zinc) when compared with state-of-the-art electrolytes, as shown in Figure 1 (cycling done at 30°C). In fact, the best cell (for Ca) demonstrated 65% capacity retention after 300 cycles at C/3 rate compared to 30% capacity retention in the baseline cell.

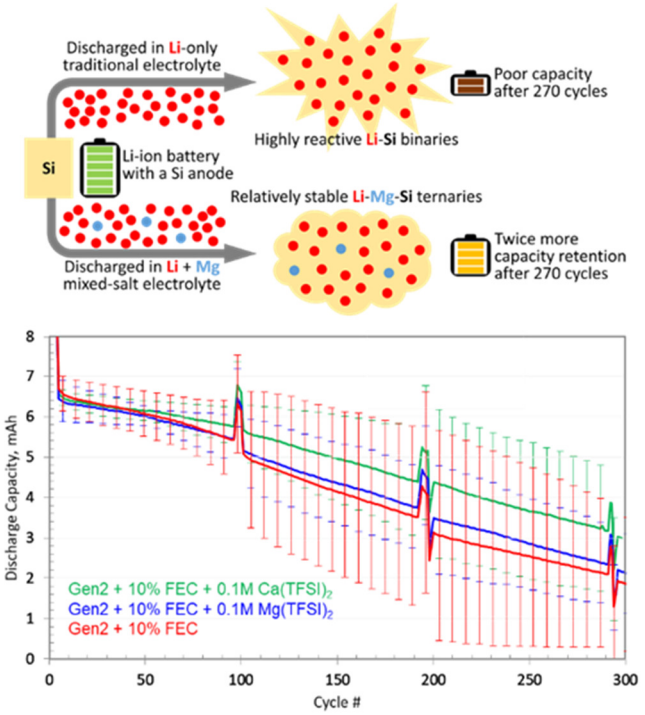

Figure 1. Effect of using mixed salt electrolytes on 7 mAh full single layer graphite free pouch cells (LMR NMC cathode against 80% Si nanoparticles with10% hard carbon 10% LiPAA binder), anodes contain no graphite.

Multiple diagnostic techniques (Bi Han, et al, & Bs Key, *ACS Applied Materials & Interfaces* 11 (33), 29780, 2019) were used to verify that adding M salts leads to the co-insertion of M cations along with Li into the Si lattice during the lithiation process, stabilizing Si anions as described in schematic, fundamentally changing the Li–Si surface chemistry while minimally affecting electrochemical profiles and storage capacity. This study opens a new and scalable way with a simple additive to stabilize Si anodes towards enabling widespread application of Si anodes in Li-ion batteries.

2019 U.S. DRIVE Highlight

High-Performance Lithium-Metal Cell Technology

The Battery500 Consortium has fabricated a 2Ah lithium metal anode pouch cell delivering 350 Wh/kg (well above industry maximum of 300Wh/kg) which achieved more than 250 cycles at room temperature with less than 5% capacity fading.

The Battery500 Consortium Core Team (Pacific Northwest National Laboratory, Brookhaven National Laboratory, Idaho National Laboratory, SLAC, Binghamton University, UC San Diego, Stanford University, University of Texas Austin, and University of Washington).

Lithium (Li)-ion batteries have found wide applications in electric vehicles and grid-scale energy storage systems, but it is difficult to further increase the energy density beyond 300 Wh/kg using graphite anodes. The Battery500 Consortium is a multi-institute program to develop next-generation high-energy and low-cost Li metal anode cells delivering up to 500 Wh/kg.

- The Battery500 Consortium deploys a multi-disciplinary strategy to use high-capacity Li metal anode, and nickel manganese cobalt oxide (NMC) or sulfur (S) cathode for high-energy cells.
- The Consortium aims to overcome fundamental scientific barriers in the fabrication and performance of pouch cells.
- The Battery500 team is made of leading scientists and engineers in the United States, including the 2019 Nobel Laureates in Chemistry, Professor Stanley Whittingham and Professor John Goodenough.
- The Consortium leverages the latest advances in battery research and state-of-the-art facilities, and implements and optimizes the most advanced electrode materials in industry relevant pouch cells.

The Battery500 Consortium has made significant progress developing electrolyte and electrode materials, and in integrating and optimizing these materials in industry relevant pouch cells.

- The team has implemented and optimized strategies for the design, fabrication and testing of high-energy pouch cells.
- The team has developed and implemented standard testing protocols, and safety procedures for cell fabricating and testing.
- The team has developed new stable electrolytes for Li-metal anodes, and optimized electrode materials and architectures for high-energy cells with lean electrolyte ratios and thin Li foil (50 microns).
- The team has developed and used advanced tools to characterize thick cathodes (4 mAh/cm^2), Li dendrite formation and pressure effects to extend cell cycling life.
- The consortium fabricated and tested 350Wh/kg Li-NMC pouch cells cycled more than 250 cycles (greater than 95% capacity retention) (Figure 1), and reduced cell swelling compared to past baselines.

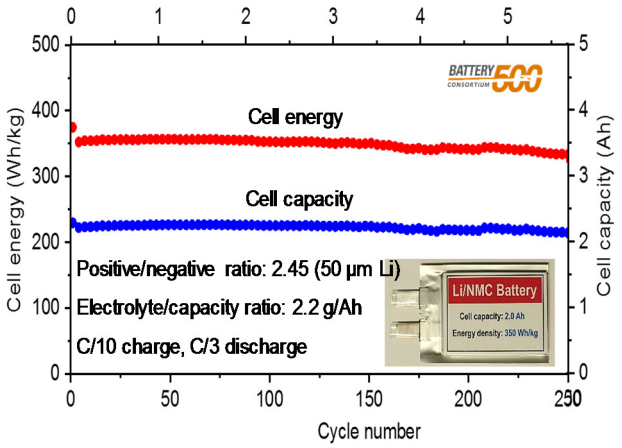

Figure 1. The whole cell capacity (blue) and the specific energy (red) of a 2.0 Ah pouch cell as a function of charge and discharge cycles. More than 90% of the cell capacity and specific energy can be retained after 250 cycles.

2019 U.S. DRIVE Highlight

Improved Performance in High-Nickel Cathodes via Surface Conditioning Synthesis Protocols

Researchers reveal how surface reconstruction occurs during the synthesis of high nickel cathodes and develop synthesis protocols to alleviate this issue, thereby improving their performance.

Brookhaven National Laboratory

High-nickel (Ni) layered oxides (with ≥70% Ni) are the most promising cathodes for lithium (Li)-ion batteries (LIBs) for electric vehicles, due to their high capacity and low cost. The high Ni loading, however, gives rise to poor cycling and rate performance. Significant efforts on developing high-Ni cathodes have focused on materials synthesis/processing, mostly on tuning the structural ordering in the bulk. However, recently researchers started to pay closer attention to surface reconstruction as evidence has been growing that this issue could lead to high impedance to Li+ (de)intercalation (Figure 1). However, it's unclear how the reconstruction occurs and how the issue should be alleviated during synthesis.

At Brookhaven National Laboratory (BNL), scientists have developed in situ techniques for real-time monitoring of synthesis reactions at various length scales. Using the capability, the BNL team studied the process of synthesizing high-Ni layered oxides by tracking intermediates and their structural (re)orderings, not only in the bulk but also at the surface. Through these efforts, BNL revealed the accumulation of lithium carbonate (Li_2CO_3), formation of a Li-deficient layer, and Ni reduction at the particle surface, as a result of the near-surface Li/oxygen loss in the final cooling stage of synthesis. The kinetic reconstruction process occurs predominantly at high temperatures (above 350°C) and is highly cooling-rate dependent.

With the findings, the BNL team has developed protocols for synthesizing high-Ni layered oxides ($LiNi_{0.7}Mn_{0.15}Co_{0.15}O_2$) with reduced interfacial impedance, improved rate capability, and higher capacity (Figure 2). Results are published in Advanced Energy Materials at: https://doi.org/10.1002/aenm.201901915.

Researchers will test the protocols in future studies in developing other high-Ni, low-cobalt (Co) or Co-free cathodes, which are of interest for next-generation LIBs.

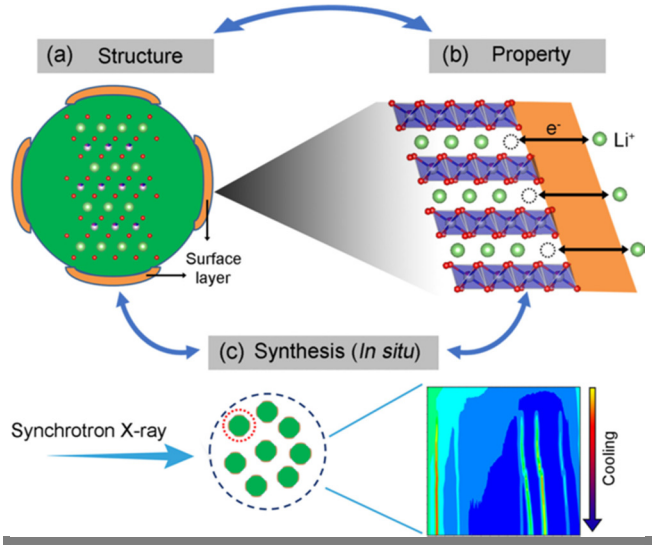

Figure 1. Schematic illustration of the approach for rational synthesis of high Ni layered oxides with a closed loop, specifically, through studying the surface reconstruction, its impact to electrochemical properties, and its formation process (using in situ synchrotron X ray techniques).

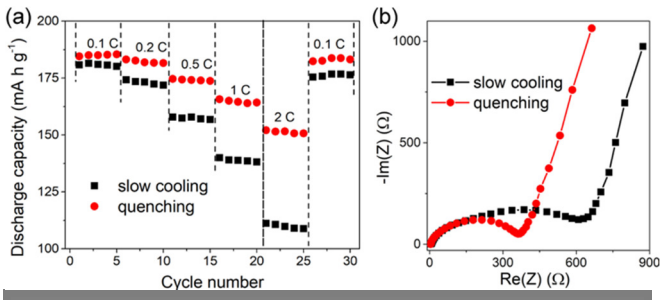

Figure 2. (a) Rate performance and (b) impedance of the $LiNi_{0.7}Mn_{0.15}Co_{0.15}O_2$ samples by slow cooling and quenching.

2019 U.S. DRIVE Highlight

Cathode Cracking Phenomena in Fast-Charging Newly Identified as a Focus Area for Durability Improvement

Under high rate charging, intergranular cracking of secondary cathode particles is found to be a potential source of major capacity fade.

Idaho National Laboratory

Enabling extreme fast-charging (XFC; charging a cell in ≤10 minutes) of lithium-ion batteries will spur the wider adoption of electric vehicles. Lithium plating at the anode is a key barrier to fast-charging, thus the scientific community is devoting significant efforts towards better understanding the lithium-plating issue and identifying solutions. However, the effects of fast-charging on the cathode have been largely unexplored.

During evaluation of cells that had been fast-charged, researchers at Idaho National Laboratory (INL) characterized the failure mechanisms that were related to both positive and negative electrodes. Using single-layer pouch cells, the lab performed extended fast-charge cycling (up to 450 cycles) at multiple charging rates. Researchers carried out comprehensive electrochemical analyses accompanied by targeted post-cycling testing to identify the central constraints of XFC.

Comparing cycle-life capacity fade and ex-situ evaluation of cathode particles following exposure to different charging rates, showed distinct and global cathode cracking (primary particle separation within the secondary particle) when cells are charged at higher C rates (Figure 1). Such cracking resulted in significant loss of access to the cathode-active material, which subsequently manifested as cell capacity loss and impedance rise. For the extreme charging conditions—10 minutes charging and less—the cathode-capacity loss (due to cracking) dominated the overall cell capacity loss in cells which did not have favorable conditions for Li plating (relatively low electrode loading, typical for high-power applications).

INL's finding highlights that, besides focusing on loss of lithium through plating, researchers need to pay attention to the positive electrode during XFC, in particular when the charging rate exceeds 6C.

Future efforts will include more detailed characterization of cracking, its evolution with cycling, a determination of when it becomes the limiting factor, incorporation of cathode-cracking into life models, and identification of ways to mitigate cracking during XFC conditions.

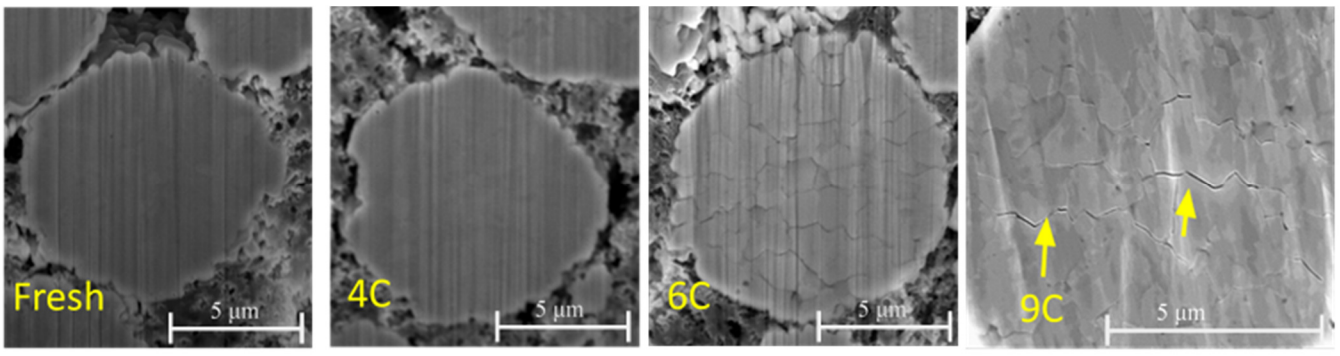

Figure 1. Scanning Electron Micrographs of secondary cathode particles (10µm diameter) show the extent of interprimary particle separation (cracking) at fresh (no fast charge cycling) and the end of cycling (up to 450 cycles) at different charging rates. A 2 hour (C/2) slow discharge was used in all cases. The cycling voltage was between 3 to 4.1 volt.

2019 U.S. DRIVE Highlight

Effect of Binder Morphology and Crystal Structure on Electrode Performance

Researchers have identified polymer structures that can lead to better or worse performance of a high energy density electrode depending upon the initial mixing and final drying conditions.

Lawrence Berkeley National Laboratory

Electrode construction can have as much of an impact on a cell's life and performance as the active material. Research is starting to shed light on how the polymer binder may play a critical role in this regard. The most commonly used binder, polyvinylidene difluoride (PVdF), takes on several forms of crystallinity depending upon the temperature at which it is formed. X-ray diffraction spectra confirms the transition of the polymer from β-phase crystallinity to α-phase when formed from slurries dried at several different temperatures. Investigating the conductivity of the films at different temperatures when wetted with an electrolyte reveal that the crystalline phase formed at lower temperatures is more ionically conductive than films formed at higher temperatures, Figure 1.

We have previously shown that the mixing order of electrode components can impact cell cycle life. We investigated drying rate and pulse power performance and discovered that electrodes prepared by mixing the active material and carbon black in solvent prior to adding a dissolved binder could be dried at temperatures up to 140°C without cracking, but electrodes prepared by mixing the carbon black with a dissolved binder prior to adding the active material could be dried as high as 180°C without cracking. However, the former process led to electrodes that dried three times faster than the latter process when dried at comparable temperatures. This suggests that the former mixing sequence leads to a polymer morphology that is thinly spread over all of the solid materials and is easily accessible for heat and mass transfer during drying whereas the latter process leads to agglomeration of conductive carbon and polymer and takes longer to dry. We also discovered that the electrodes produced with a thin layer of polymer over the active material relied on the conductivity of the film to enhance performance (Figure 2.a), whereas binder agglomerated with carbon may rely on strong mechanical properties between particles for better performance (Figure 2.b).

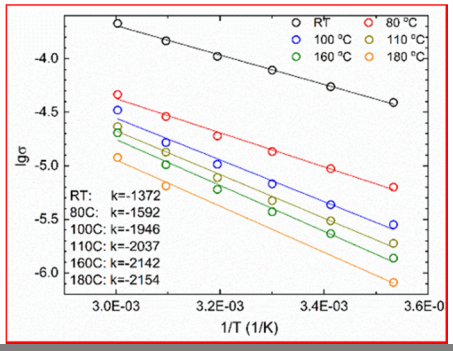

Figure 1. Log log plot of room temperature conductivity data versus inverse of the absolute temperature during drying.

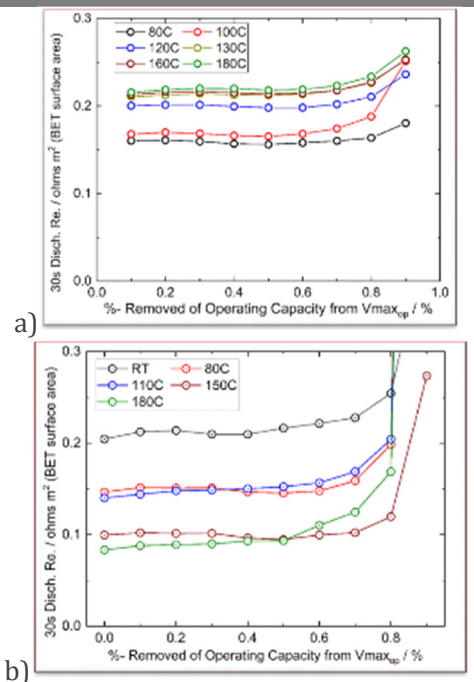

Figure 2. Resistance versus depth of discharge for electrodes dried at different temperatures a) active material and carbon black mixed together first; b) carbon black and polymer slurry mixed together first.

2019 U.S. DRIVE Highlight

Freeze Casting Innovation for Composite Cathode Architectures in All Solid-State Lithium Batteries

The first demonstration of a solid state battery with a thick composite electrode based on LLZO impregnated with layered transition metal cathode

Lawrence Berkeley National Laboratory, Montana State University and Mercedes-Benz Research & Development, North America

For the first time, researchers have demonstrated fully functioning bulk-type all-solid-state full cells. These cells use a composite positive cathode, and aluminum-substituted $Li_7La_3Zr_2O_{12}$ (LLZO) as the solid electrolyte. The devices incorporate bilayers composed of dense LLZO membranes and porous LLZO scaffolds infiltrated with $LiNi_{0.6}Mn_{0.2}Co_{0.2}O_2$ (NMC-622) and other components as the cathode, combined with lithium (Li)-metal anodes. The porous scaffolds are prepared using a scalable freeze-tape-casting method. The unidirectional pores of the scaffold facilitate infiltration of cathode components and shorten Li-ion diffusion path-lengths, while the addition of a soft ionically conductive solid (succinonitrile [SCN]) to the scaffold ensures good contact among the components (Figure 1).

To the best of our knowledge, this is the first report of successful room temperature cycling of a bulk and truly all solid-state battery (ASSB) using a LLZO separator and composite electrode in a practical form factor. Examples of LLZO thin films or bilayer/trilayer architectures involving a thin LLZO layer have been reported previously. However, the constructed cells all use liquid electrolytes to address the cathode/LLZO interfacial contact issue and are therefore not truly solid state. In addition, almost all studies reporting solid-state batteries use thick LLZO pellets (3-5 mm) and apply/attach active materials to complete a cell. While those studies are useful for answering fundamental questions, they are not in a practical form factor. The use of thick pellets and thin cathode layers greatly compromises energy density. The LLZO should be in a thin film form, to minimize weight and volume as well as impedance.

In this work, the LLZO separator thickness was 36 microns, and the porous LLZO structure containing the cathode material was 140 microns and 4-5 mg/cm² of active cathode material (https://dx.doi.org/10.1021/acsaem.9b02101). The superior electrochemical performance (constructed devices had impedances of 350 Ω cm² compared to cells with no SCN-based solid electrolyte infiltration, which had impedances of 180,000 Ω cm²) can be ascribed to several factors including using a thin, dense LLZO separator layer; seamless Li/LLZO contact; a low tortuosity pore structure; and intimate contact among the components in the composite cathode structure.

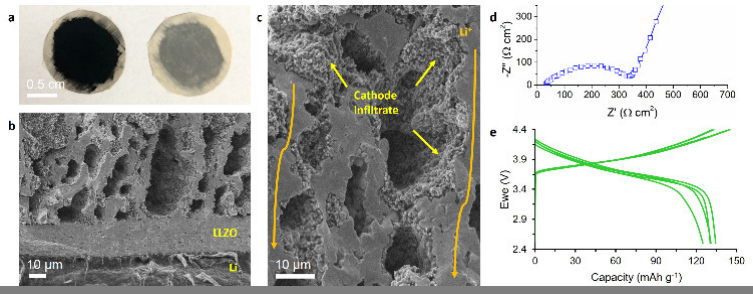

Figure 1. (a) Optical image of cathode infiltrated LLZO bilayer. Cathode infiltrated porous layer surface (left) and dense layer surface (right) are shown. (b) Scanning electron microscopy fracture surface image of cathode infiltrated bilayer. Images were taken prior to SCN electrolyte infiltration. (c) Same cell at higher magnification showing cathode infiltrate. (d) Nyquist plot of the constructed ASSB. (e) Initial charge/discharge profiles of the ASSB.

2019 U.S. DRIVE Highlight

Surface Dopants to Stabilize High-Nickel Cathodes

Alleviating capacity fade and impedance rise due to oxygen release from lithium nickel oxide using theory guided screening of surface dopants.

Lawrence Berkeley National Laboratory

Layered transition-metal oxides remain the majority of the cathode materials in commercialized lithium-ion batteries (LIBs). To further increase the energy density and decrease the reliance on cobalt, the nickel (Ni) content in the current Ni-rich cathodes has been progressively increased. However, deteriorating cycling performance currently limits widespread deployment. One major culprit is oxygen (O) loss, which increases surface impedance and undermines the thermal stability of LIBs.

Lawrence Berkeley National Laboratory (LBNL) has used theory-guided screening to discover a number of surface dopants that alleviate O evolution from lithium nickel oxide ($LiNiO_2$). To evaluate each dopant's ability to suppress the surface O loss, we calculated the relative O release energy during delithiation of doped-$LiNiO_2$ with respect to the pristine phase (Figure 1a). Figure 1b shows a surface model of doped-$LiNiO_2$ (104) surface facet. It was found that the calculated O release energies of antimony (Sb)-, tantalum (Ta)-, and titanium (Ti)-doped $LiNiO_2$ are higher than that of the pristine phase, which implies that Sb, Ta, and Ti can enhance the surface O retention of $LiNiO_2$, and Sb is predicted to be the most promising.

Further insight into the nature of the dopant-O bonding is provided by an electron localization analysis, Figure 1c. The green regions between the Sb and O atoms correspond to shared electrons, a signature of covalent bonding. Therefore, a higher degree of electron sharing between Sb and O leads to a stronger Sb-O bond and better O retention.

Finally, the team at LBNL is working with experimental collaborators from Virginia Tech University to verify the predictions. The initial results show an improved capacity retention in 2% Sb-doped $LiNiO_2$ over the pristine phase, Figure 1f and g.

In summary, Sb, Ti, and Ta were identified as promising dopants to mitigate surface O loss from $LiNiO_2$. The effectiveness of Sb doping was rationalized based on the bond strength between the dopant and O.

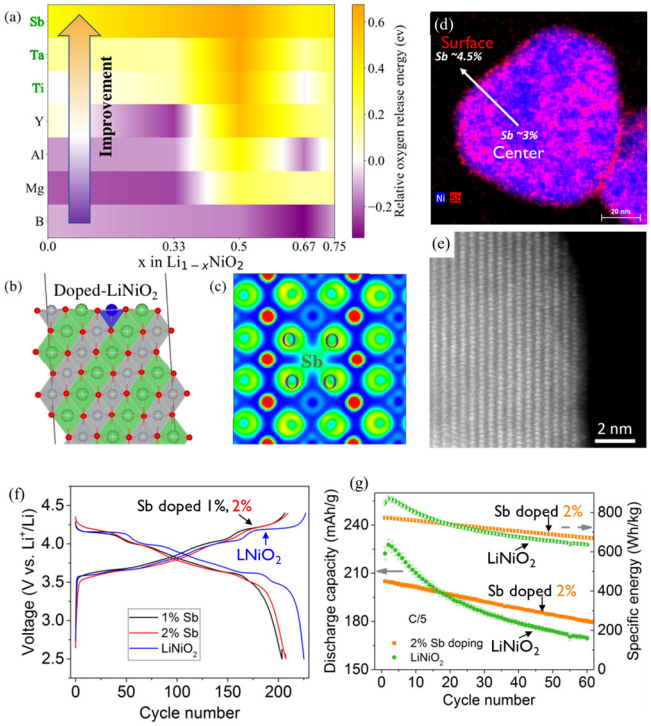

Figure 1. (a) The relative surface O release energies of doped $LiNiO_2$ with respect to the pristine phase. Yellow orange indicates an improved O retention, while purple indicates a reduced O retention compared to the pristine phase. (b) Schematic illustration of surface doped $LiNiO_2$ model. Blue: dopant, green: Li, grey: Ni, red: O. (c) 2D electron localization function contour plot for the surface of Sb doped $LiNiO_2$. (e) transmission electron micrograph of Sb doped $LiNiO_2$ with no surface reconstruction. (f) Initial charge/discharge curves at C/10 rate of undoped and doped $LiNiO_2$. (g) ½ cell cycling data at C/5 rate showing reduced fade of Sb doped $LiNiO_2$.

2019 U.S. DRIVE Highlight

Zero-Strain Layered-Rocksalt Intergrown Cathodes for Future High-Energy Density Cell Development

Layered rocksalt intergrown oxide cathodes can harness the high capacity of layered and rocksalt phases, good kinetics of layered oxide, and isotropic structural advantages of the rocksalt phase.

Lawrence Berkeley National Laboratory

Lithium (Li)-rich metal oxides of layered and rocksalt structure with a high capacity (250-300 mAh/g) are promising candidates for high-energy Li-ion cathodes. Although both materials share a similar close-packed oxygen framework, layered oxide cathodes suffer from an irreversible phase transformation as well as oxygen loss at high voltage (leading to energy fade and impedance rise), while rocksalt oxides typically do not cycle Li but exhibit a minimal isotropic structural change upon cycling. It would be ideal to harness the combined figures of merit from each phase. So far, limited success has been demonstrated to utilize the structural compatibility of layered and rocksalt phases for the development of high-performance Li-ion cathodes.

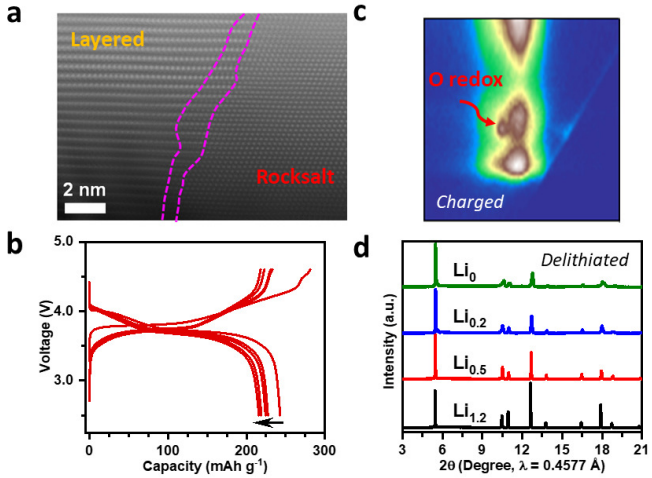

Figure 1. (a) Representative HAADF STEM image of $Li_{1.2}Ni_{0.4}Ru_{0.4}O_2$, showing the layered rocksalt intergrown structure along the [110] axis; (b) charge discharge voltage profiles during the first five (C/50) cycles of a ½ cell; (c) O *K* edge resonant inelastic X ray scattering map at charged state, red arrow indicating the fingerprinting feature of oxidized oxygen; and (d) X ray diffraction patterns of $Li_xNi_{0.4}Ru_{0.4}O_2$ (x 1.2, 0.5, 0.2, 0) at different delithiated states, showing the isotropic structural evolution upon delithiation.

At Lawrence Berkeley National Laboratory, we propose a concept of layered and rocksalt intergrown structures for advanced Li-ion cathodes. For the proof of concept, we designed and synthesized lithium nickel ruthenium oxide, $Li_{1.2}Ni_{0.4}Ru_{0.4}O_2$, which exhibits a main layered $R\bar{3}m$ structure with well-grown rocksalt $Fm\bar{3}m$ nanodomains that are introduced to stabilize the electrochemically active layered structure. High-angle annular dark-field scanning transmission electron microscopy (HAADF-STEM) images (Figure 1(a)) reveal an intergrown structure with the rocksalt domain embedded in the main layered phase. This layered-rocksalt intergrown oxide displays an initial capacity of 244 mAh/g, almost 90% of the total theoretical capacity.

We then further probed the phase evolution of layered-rocksalt intergrown oxides upon electrochemical cycling. There is no new phase formation upon the extraction of Li^+. Strikingly, the lattice parameters *a* and *c* of the layered $R\bar{3}m$ component exhibit an isotropic change. It is worthwhile noting that both lattice parameter *a* and *c* of the layered $R\bar{3}m$ component show a minimal change of ~1%, hence referred to as "zero-strain" electrode. The layered-rocksalt intergrown phase displays an excellent structural robustness with a minimal change in lattice parameters upon delitiation/lithiation. Although ruthenium is too expensive to be widely used in an automotive battery, the success of such layered-rocksalt intergrown structure demonstrates a new concept of cathode design and opens up a vast space of compositions to develop high-performance intergrown cathodes for advanced energy storage devices.

2019 U.S. DRIVE Highlight

Cobalt-Free Cathode Synthesis, Scale-up, and Performance

Researchers are mitigating potential cobalt supply and cost risks by using novel cathode compositions aimed at replacing cobalt with low cost and abundant constituents.

Oak Ridge National Laboratory

Commercial cathode materials used in lithium (Li)-ion batteries such as $LiNi_xMn_yCo_zO_2$ (NMC) and $LiNi_xCo_yAl_zO_2$ (NCA) contain cobalt. Recently, cobalt prices have undergone rapid fluctuations and have nearly tripled in the last decade. This has become a risk management issue both for the battery manufacturing industry and for vehicle manufacturers, especially at a time of major electric vehicle (EV) market growth. The availability and cost of cobalt is a potential problem which may slow or reduce the future availability of renewable energy storage and EVs.

To address this challenge, researchers have embarked on developing novel classes of cobalt-free cathodes that contain low-cost constituents aimed specifically at replacing the cobalt in conventional NMC- and NCA-type cathodes. The developed cobalt-free chemistries would facilitate seamless integration into existing global battery manufacturing factories without compromising material and electrochemical performance metrics. In this context, our team has developed a new class of nickelate cathodes, composed of Li, iron, and aluminum nickelate ($LiNi_xFe_yAl_zO_2$), termed the NFA class of cathodes. Our team initially synthesized these materials using the sol-gel process to quickly explore their compositional landscape. Specific compositions starting with 80% nickel content (NFA Gen-1) and with the other constituents a combination of iron and aluminum that were selected after evaluation of their compositional and crystallographic purities. These were determined using multiple characterization techniques such as inductively coupled plasma-mass spectrometry, X-ray diffraction, and neutron diffraction; following which electrochemical evaluations were carried out. The best performing composition was down-selected for scale-up through a coprecipitation process using a continuous stirred tank reactor (CSTR). The NFA cathode particles synthesized using the CSTR are shown in Figure 1(A). The half-cell performance of the cathode is shown in Figure 1(B); it delivers a capacity of 180 mAh/g at C/3 in the voltage range of 3 volt (V)-4.5V. This is comparable to today's state of the art cobalt-containing cathodes and is promising initial performance.

The insights developed through our work highlight the potential of cobalt-free cathode materials such as NFA to provide a commercially viable pathway towards successful development of next-generation EVs with reduced cost, reduced supply chain risk, and reduced global strategic material concerns.

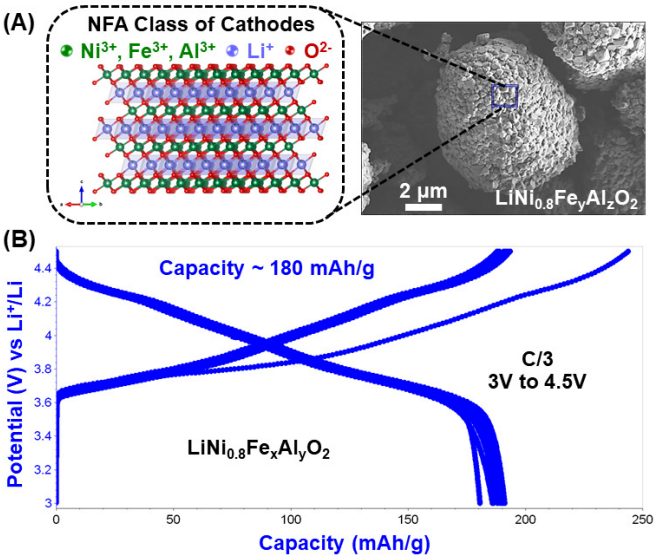

Figure 1. (A) NFA cathode particles synthesized through a co precipitation reaction in a CSTR and (B) charge/discharge curves indicating the good capacity and performance delivered by the NFA cathode material.

2019 U.S. DRIVE Highlight

Cathode Electrode Structuring with CoEx Printing Improves Performance of Thick Electrodes

By using a specially designed printhead, we demonstrate the high speed preparation of thick, patterned cathode electrodes with improved energy and power density.

Palo Alto Research Center, Oak Ridge National Laboratory, and Ford Motor Company

There is a fundamental trade-off between power and energy density in lithium (Li)-ion batteries. Higher power can be achieved with thinner electrodes, which reduces the distance that Li ions need to travel in the battery. However, thinner electrodes mean more electrode layers to achieve the same capacity, which means more inactive layers such as current collectors, which reduces energy density. Thus, one way to improve energy density is to increase the thickness of the electrode layers to reduce inactive layers, but this increases transport distances for Li ions, which limits how fast energy can be withdrawn from the electrode.

Palo Alto Research Center's CoEx printing technology is a method for depositing finely patterned films onto the current collectors used in battery manufacturing. It is designed as a drop-in replacement for slot die coating, the predominant technology used for producing battery electrodes, with comparable throughput and similar slurry formulations. The purpose of this collaboration is to demonstrate the effectiveness of CoEx structuring at the coin cell level, and then scale up printhead and processing to produce 1 Ah and 10+ Ah pouch cells.

Figure 1 is a cross-section of a typical CoEx electrode after printing and drying. The structuring process results in periodic fine grooves along the length of the electrode, which get filled with electrolyte during assembly and provide enhanced ionic transport paths. Figure 2 shows a comparison of CoEx electrodes to thick, conventionally prepared cathode electrodes. Even though the CoEx electrodes are of similar thickness and loading, they perform much better at greater than C/2 discharge rates.

Table 1 shows the improvement in energy density between CoEx and conventional cathode electrodes in larger format (15–17 Ah) pouch cells. The improvement in battery performance is most evident at ≥ 1C discharge rates.

CoEx printing is thus a promising means to engineer battery electrodes and thus achieve both high energy (high loading) and high power simultaneously.

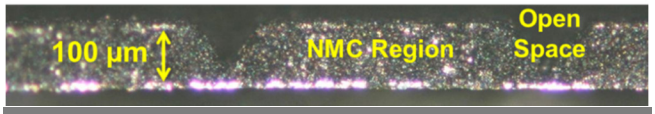

Figure 1. Optical cross section of CoEx electrode after printing and drying. Periodic grooving provides improved transport paths for ion flow.

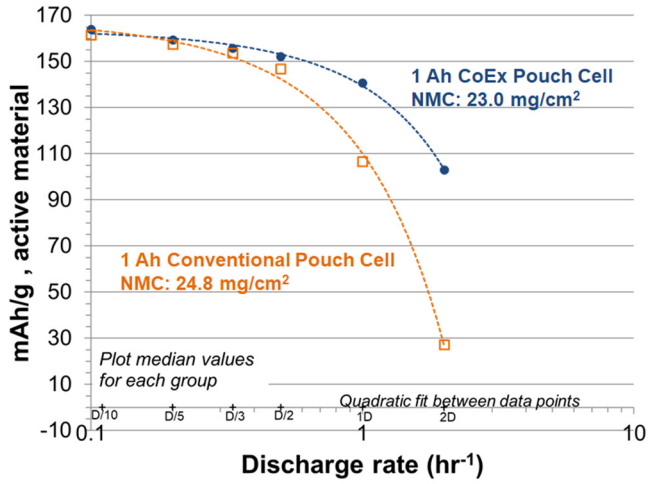

Figure 2. Comparison of specific capacity between CoEx cells and conventional cells in 1 Ah format.

Charge time (1/ D rate)	Wh/L	Wh/kg
10 hours	1	0
1 hour	3	3
12 minutes	94	93

Table 1. Improvement in energy density of CoEx over conventional cells (%).

2019 U.S. DRIVE Highlight

Maximizing Fast Charging of Lithium-Ion Batteries via Real-Time Detection of Lithium Plating

High precision characterization techniques allow early detection of lithium plating and provide the ability to rapidly assess the fast charge capability enabled by anode improvements.

Sandia National Laboratories[1]

Fast-charging of lithium (Li)-ion batteries is a critical enabler for mass electric vehicle (EV) adoption. Sandia National Laboratories (SNL) has been working with the University of Michigan to develop graphite anodes with novel three-dimensional structures that facilitate faster charging while avoiding Li plating, a main danger of improperly controlled fast-charging. SNL is using its unique high precision cycling capability to characterize the ability of improved anodes to withstand fast charge and avoid Li plating.

SNL has observed discrete signals related to Li plating at increased charge rates, using a technique called differential coulometry, which benefits from our high precision cycling capability. Figure 1 shows differential coulometry plots for battery charging at increasing rates (light blue to dark red). The 2.85 Ah pouch cell contained a standard graphite anode with no improvements. The cell had an automotive-relevant energy density of 200 Wh/kg.

At low charge rates (2-hour charge), peaks from 3.5-3.8 volt (V) indicate normal charging behavior. At higher rates (20 min charge), a second growing peak at 4.1V indicates a new process occurring, which is believed to be Li plating. Such an observation allows real-time identification of Li plating behavior, including at what current it occurred, and to what degree. With the ability to identify the very earliest signs of Li plating (Figure 2), a powerful tool is available to compare batteries using present day unimproved anodes, with batteries containing advanced 3D structured anodes. Using this tool, our project aims to deliver batteries with the ability to charge in as quickly as 10 minutes.

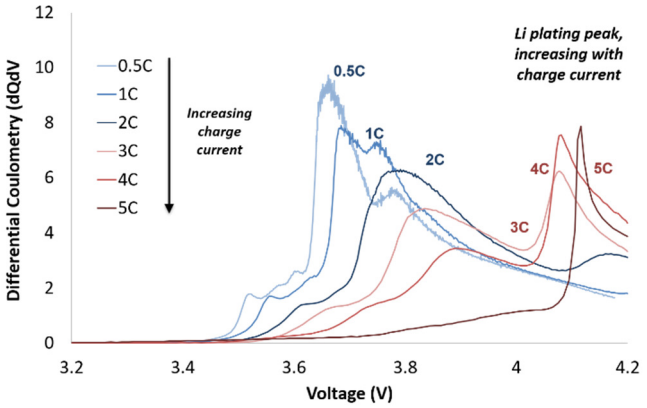

Figure 1. Differential coulometry (dQ/dV) of charge steps.

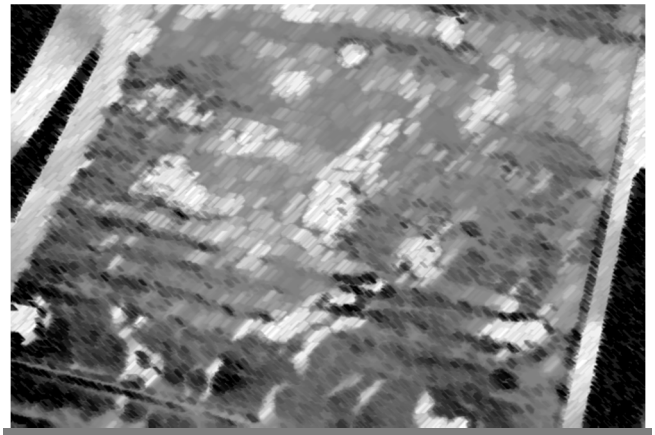

Figure 2. Cell teardown picture of standard graphite anode with clear evidence of plated Li.

[1] *Sandia National Laboratories is a multimission laboratory managed and operated by National Technology and Engineering Solutions of Sandia, LLC., a wholly owned subsidiary of Honeywell International, Inc., for the U.S. Department of Energy's National Nuclear Security Administration under contract DE-NA-0003525.*

Fuel Cells

2019 U.S. DRIVE Highlight

Performance and Durability Models Highlight Path to Reaching DOE Targets

Argonne s modeling efforts identified improvements needed to achieve U.S. Department of Energy targets.

Argonne National Laboratory

A validated fuel cell model that can predict how variations in operating conditions, electrode design, and catalyst design impact performance, cost, and durability is a valuable tool for research and development activities and for identifying opportunities for further improvements. Argonne National Laboratory (ANL) has developed and validated a model for automotive Proton Exchange Membrane fuel cell systems using data from U.S. Department of Energy (DOE)-funded projects and input from a wide range of stakeholders. The model plays a primary role in assessing component performance in an integrated system, optimizing operating conditions for performance and cost, supporting DOE in setting targets and directing component development, and providing data and specifications for the annual manufacturing cost update.

In the past year, ANL modeled performance and degradation of a platinum group metal free (PGM-free) catalyst and determined what improvements would be necessary to meet DOE fuel cell performance targets. The model indicates improvements are needed in catalyst activity and in the electrode structure to reach the target power density of 1W/cm² stack cost equivalent while meeting the heat rejection target (Figure 1). The PGM-free catalyst mass activity would need to improve by 12X, while also increasing active site density by a factor of two. In addition, improvements are needed in electrode design to decrease thickness to ½ current electrodes to decrease mass transfer losses. The large improvements needed suggest platinum (Pt)-based catalysts will be used to achieve the near-term DOE targets for automotive applications.

ANL also developed durability models for state-of-the-art Pt and platinum-cobalt (PtCo) catalysts that include the effects of aging on the electrode structure, the kinetics of the oxygen reduction reaction, and the oxygen mass transport resistance as a function of potential cycles and relative humidity. These studies determined that 40% of the loss in mass activity of state-of-the-art PtCo catalysts after 30,000 potential cycles was due to Co dissolution, while 60% of the loss was due to growth in particle size. To keep the loss in power density at rated power to the 10% target, the modeling indicates that electrochemical surface area losses must be kept below 40%.

ANL modeled fuel cell systems for heavy-duty truck applications, investigating the impact of Pt loading on performance and durability and looking at heat rejection requirements for highway cruising and a hill climb at 6% grade. Initial results indicate that high Pt loadings (up to 0.4 mg/cm²) and battery hybridization may be needed to meet the heat rejection and durability requirements.

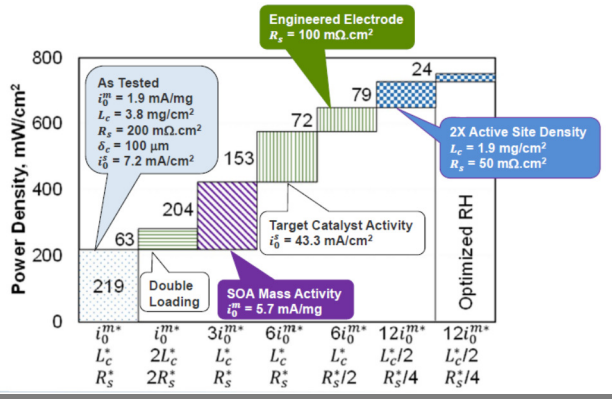

Figure 1. Systematic improvements needed in PGM free catalyst activity and electrode structure to reach 770 mW/cm² power density.

2019 U.S. DRIVE Highlight

Platinum-Gold Alloy Cathode Catalyst Achieves 3x Stability

Active, durable catalyst developed to reduce fuel cell cost substantially.

Argonne National Laboratory

The cost of platinum (Pt)-based cathode catalysts at loadings necessary to achieve the required performance and lifetime is one of the main contributors to fuel cell system cost. Argonne National Laboratory, with project partners the National Renewable Energy Laboratory and Oak Ridge National Laboratory, have developed a Pt-gold (PtAu) catalyst that could substantially decrease the amount of Pt needed to achieve fuel cell lifetime targets, thus reducing cost. The new catalyst shows high oxygen reduction reaction (ORR) activity and superior catalyst activity retention compared to state-of-the-art Pt after 30,000 cycles of the U.S. Department of Energy's catalyst accelerated stress test (Figure 1).

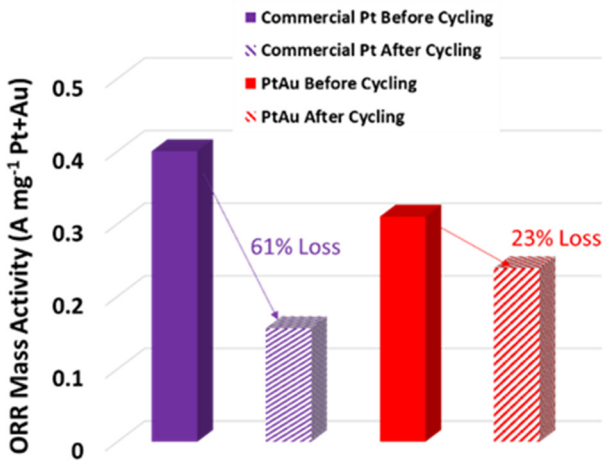

Figure 1. Comparison of the PtAu catalyst s mass activity in a fuel cell with that of conventional Pt/C, before and after potential cycling.

The PtAu catalyst stability was achieved through the formation of a thin Pt skin on a PtAu alloy core, as shown in the energy dispersive X-ray image in Figure 2 (Top). Advanced characterization, including on-line inductively-coupled plasma mass spectrometry and ultra-high vacuum techniques, has revealed the mechanism of catalyst degradation by Pt dissolution and means for fully preventing Pt dissolution in fuel cells. Based on these fundamental studies, PtAu was developed to completely suppress the dissolution of Pt from the skin by Au in the particle core (Figure 2 (Bottom)) and by synthesis of catalyst particles with uniform size. Next steps include optimizing the catalyst for higher activity and demonstrating fuel cell performance under all relevant operating conditions.

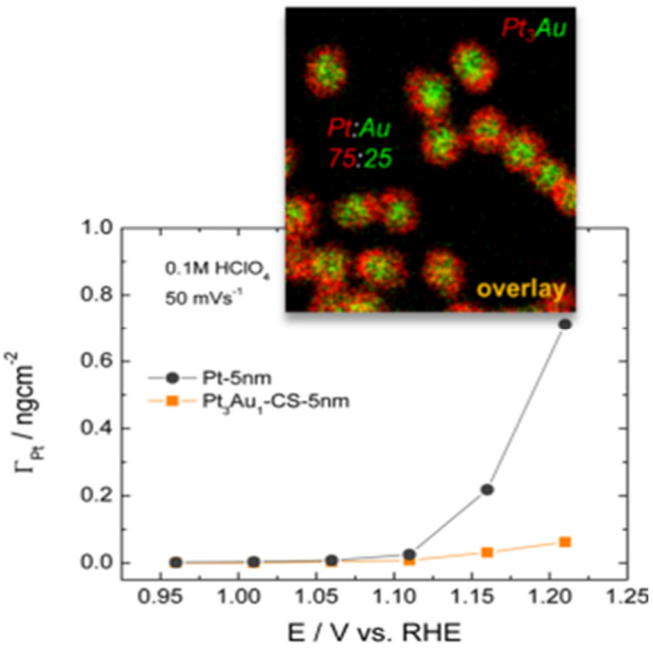

Figure 2. (Top) Distribution of Pt and Au in monodisperse 5 nm PtAu nanoparticles and (Bottom) Suppression of Pt dissolution from PtAu particles.

2019 U.S. DRIVE Highlight

Characterization of a Fuel Cell Electrode Transport

Improved understanding of reactant and cation transport in fuel cell membrane electrode assembly through experiment and modeling.

FC-PAD: Fuel Cell Performance and Durability Consortium

FC-PAD, a National Laboratory-based consortium established by the U.S. Department of Energy's Office of Energy Efficiency and Renewable Energy, Fuel Cell Technologies Office to improve fuel cell performance and durability, pursued detailed materials analysis on fuel cell membrane electrode assemblies (MEA). Better understanding of the structure-function relation of the MEA can lead to smaller fuel cell stacks and overall cost reduction.

State-of-the-art MEAs often disperse platinum (Pt) catalysts on high-surface-area-carbon (HSC) supports in the cathode electrode to maximize Pt utilization toward converting gaseous oxygen (O_2) to water. The non-uniform nature of the Pt/HSC and ionomer composite electrode makes understanding of the performance and durability difficult. The FC-PAD consortium utilized various imaging and spectroscopic techniques to reveal the material composition and structure of the cathode. Additionally, simulation during the O_2 reduction reaction using the microscale transport-catalyst layer agglomerate model helped articulate O_2 transport and water accumulation within the catalyst agglomerates. The model shows how the morphology of the agglomerates causes localized liquid water condensation (Figure 1). Although the liquid water facilitates proton transport to internal Pt particles, it hinders O_2 transport if it becomes excessive. This provides a foundation for designing better fuel cell electrodes.

Another key accomplishment is a collection of studies to help understand the effect of cation (Co^{2+}, Ce^{3+}) on fuel cell performance (Figure 2). Cations replace protons and decrease proton conductivity. Because cations are mobile, their effect on performance is difficult to predict. FC-PAD performed a range of transport related measurements and then applied both dilute and concentrated solution theories to reveal how cations can affect the proton transport in ionomer. This helps explain why some cations cause more performance loss than others and will lead to a better fuel cell design. In-situ observation of cations in the MEA using FC-PAD's synchrotron X-ray capability also provide means to understand the interaction of fuel cell operating parameters on the mobility of cations and fuel cell performance.

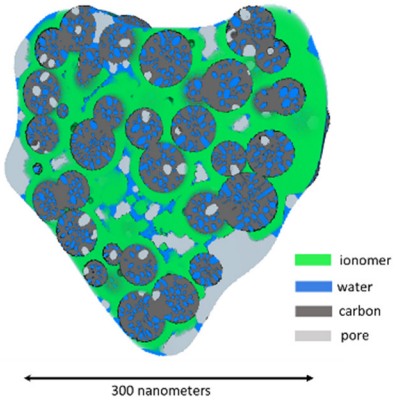

Figure 1. Cross sectional schematic of a cathode agglomerate model, reconstructed from X ray tomography, showing condensed liquid water at 84% relative humidity.

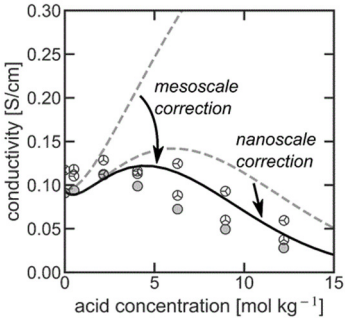

Figure 2. Effects of mesoscale (water uptake, tortuosity) and nanoscale (viscosity) on proton conductivity according to concentrated solution theory are used in development of the cation performance model.

Improved High-Power Performance of Fuel Cell Catalyst

Ordered intermetallic platinum and cobalt alloys on accessible carbons enhanced the performance and durability at high current density.

General Motors

The performance and durability of fuel cell catalysts, especially at high current density, have a direct impact on the cost of fuel cell vehicles. The General Motors-led project, supported by Cornell University, developed ordered intermetallic platinum (Pt) and cobalt (Co) alloy catalysts dispersed on engineered accessible carbon supports. The team boosted platinum group metal (PGM) utilization and high current density performance, to levels exceeding the U.S. Department of Energy's (DOE) target (Figure 1). The catalysts with low Pt loading (0.075-0.125 mgPt/cm^2) improved performance at both low and high current densities, as well as increased catalyst durability, all passing DOE's 2020 targets.

The project studied local transport of gases and water using electrochemical diagnostics, microscopy, and simulation, enabling identification of an ideal porous structure of the carbon support. The team optimized the PtCo-particle-size for improved metal stability in the catalysts. The project also developed a process to apply ionic liquids (IL) in the membrane electrode assemblies (MEA) to improve the electrode proton conduction and Pt utilization under dry conditions. The IL thin film on the catalyst layer increased the Pt surface area and oxygen reduction reaction retention during catalyst durability testing. The team also developed a catalyst aggregate model based on microscopy data to simulate oxygen and proton transport in the catalyst layer. The modeling confirmed that optimized internal pore size is the key factor determining the catalyst utilization.

Remaining challenges include optimizing IL dispersion on the intermetallic alloy catalysts and the accessible-porous carbon supports in MEA to improve the high current density durability. This work could also enable the application of the fundamental understanding of the high-power performance catalyst with ultra-low Pt loading to help design catalysts with higher Pt loadings for heavy-duty trucks application.

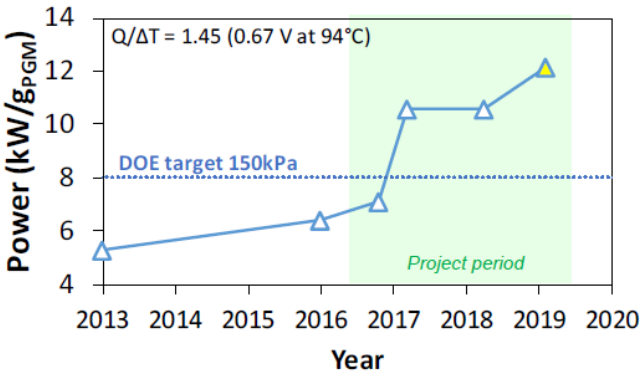

Figure 1. Improved power performance of the catalysts that exceeded the DOE target.

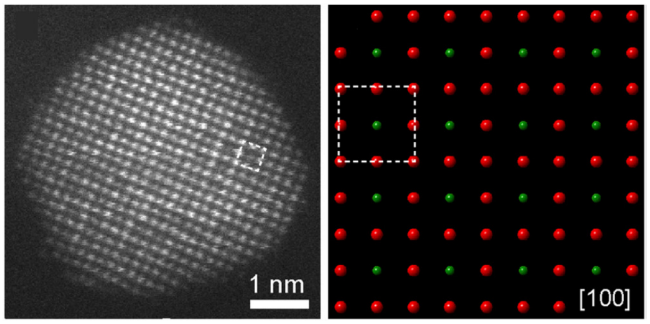

Figure 2. (Left) A partially ordered intermetallic particle on the [100] zone axis. Both brighter and dimmer atoms exist at the center of the squares. (Right) Corresponding projected crystal model along [100]. Red and green atoms are Pt and Co, respectively.

Hydrogen Storage

2019 U.S. DRIVE Highlight

Leveraging Cooperative Materials Development Efforts to Reduce the Cost of Hydrogen and Natural Gas Storage

A new collaborative effort with the Vehicle Technologies Office focuses on materials development strategies to reduce the costs of onboard vehicular hydrogen and natural gas storage.

Fuel Cell Technologies and Vehicle Technologies Offices

The Hydrogen Storage Program initiated a collaborative effort between DOE's Fuel Cell Technologies (FCTO) and Vehicle Technologies Offices (VTO) to reduce the cost of both onboard hydrogen (H_2) and natural gas (NG) storage. Similar to 700 bar H_2 tanks for fuel cell electric vehicles (FCEVs), the high cost of compressed natural gas (CNG) tanks impedes increased deployment of natural gas vehicles (NGVs). The most significant component cost difference between a heavy-duty CNG truck and an equivalent diesel truck is the fuel storage system (Figure 1).[2] This is largely due to the carbon fiber composite used in high pressure (250 bar) CNG tanks.

To address this challenge, FCTO and VTO have leveraged resources to fund a joint program comprising of seven projects developing a variety of low-pressure materials-based gas storage solutions. FCTO has a long history of funding materials-based H_2 storage research and will lead the combined effort through its Hydrogen Materials—Advanced Research Consortium. Developing materials-based gas storage would enable storage tank pressures of 100 bar or lower, reducing the cost of both types of tanks and infrastructure costs; it will also reduce energy consumption by minimizing compression costs at refueling stations.

While DOE-supported R&D has improved the state-of-the-art for gas adsorbents, significant challenges remain to achieve commercial targets. Improvement strategies for NG and H_2 adsorbents share many common goals; this collaboration will leverage FCTO's experience with H_2 storage to solve problems hindering the increased deployment of NGVs.

One common goal for both types of adsorbents concerns the inherent low packing density of solid materials. Inefficiencies in how adsorbent particles fill a tank can result in large differences between the amount of gas a material can hypothetically store and what can be achieved in a realistic system. Past work has shown that many adsorbents are not amenable to traditional densification methods.

Another strategy to improve both NG and H_2 adsorbents is reducing the difference between how much gas a material can store at the charging pressure (total capacity) vs. how much gas the material can deliver to power the vehicle (usable capacity). This difference arises because both NGVs and FCEVs require at least 5 bar of gas pressure to operate. Therefore, any gas adsorbed by the material below this minimum pressure is not utilized.

Collaborative work using flexible adsorbents to increase the usable capacity problem, and a newly discovered monolith method to attack the packing density problem, could make these technologies affordable. By coordinating the CNG and H_2 efforts, the Program hopes to accelerate deployment of both new, clean-energy technologies into the market.

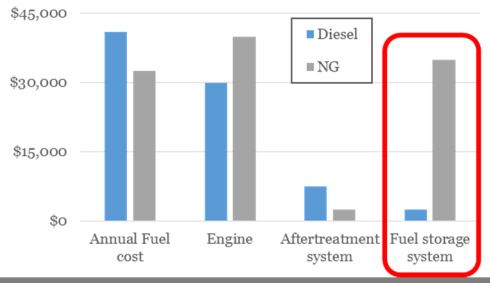

Figure 1. Selected component costs for diesel and NG heavy duty Class 8 trucks, based on 100,000 miles/year and current fuel prices.

[2] Curran, S. et al, *Comparative Analysis of Differentiating Technology Cost Components for NG vs Competing Options for Medium-Duty and Heavy-Duty Trucks*. ORNL/TM-2019/1202.

2019 U.S. DRIVE Highlight

Cost of a 700 bar Type IV Hydrogen Storage System Significantly Reduced

Type IV compressed hydrogen storage system cost is projected to be 30% lower than the 2013 baseline.

Strategic Analysis, Inc. and Argonne National Laboratory

Cost analysis performed by Strategic Analysis, Inc. (SA) projected a ~30% net reduction in the cost of a 700 bar Type IV (polymer liner and carbon fiber composite overwrap) onboard hydrogen storage system compared to the 2013 baseline estimate. As illustrated in Figure 1 and documented in a new DOE Program Record, the high volume cost at 100,000 units per year was reduced from $22.1/kWh (~$4,100) in 2013 to $15.7/kWh (~$2,900) in 2019 (assuming a single tank system with 5.6kg usable hydrogen storage capacity).[3]

Argonne National Laboratory (ANL) conducted modeling of the pressure vessel to optimize the performance using finite element analysis. SA projected the system level cost based on advancements in material and design assumptions using Design for Manufacture and Assembly®, a process-based methodology which projects material and manufacturing costs of the complete system by summing the costs of each manufacturing step.

The primary advancements leading to the 30% cost reduction include:

- Development of a lower cost polyacyrlonitrile - methacrylate co-monomer carbon fiber (CF) precursor that is produced through a high-volume textile processing technique,
- Integration of the balance of plant (BOP) into the pressure regulator block body to reduce BOP parts and associated piping and fittings,
- Employing a hoop-intensive CF winding pattern that concentrates hoop windings in the interior layers to reduce complex, helical windings and overall CF composite mass,
- Development of low cost, low density, vinyl ester resin with improved mechanical properties over the conventional epoxy resin, and
- Replacing stainless steel BOP components with aluminum to reduce material and manufacturing costs.

While a 30% cost reduction since 2013 is significant, further cost reductions are still necessary in order to achieve the U.S. DRIVE 2025 hydrogen storage system goal of $9/kWh. Considering CF still accounts for more than 50% of the total system cost, additional research and development related to CF will be pursued to achieve the target.

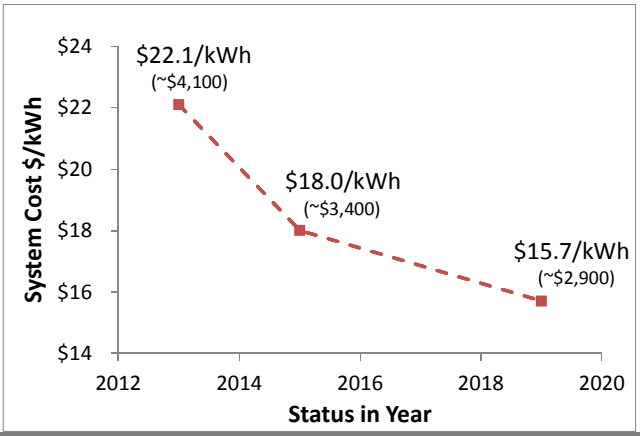

Figure 1. Projected cost reduction of 700 bar Type IV hydrogen storage system from 2013 to 2019 based on annual production rate of 100,000 units (in 2016 dollars).

[3] *2019 DOE Hydrogen and Fuel Cells Program Record*, https://www.hydrogen.energy.gov/pdfs/19008_onboard_storage_cost_performance_status.pdf.

Materials

2019 U.S. DRIVE Highlight

Graphene-Based Solid Lubricants for Automotive Applications

Development of solid lubricants for hot stamping applications.

Argonne National Laboratory

Stamped components typically account for 30%–35% of total mass of typical passenger vehicle. The body-in-weight chassis and closure components define structural integrity of the vehicle characterized by stiffness, durability, safety, ride, and handling parameters. Materials selection and design efficiency greatly impact the safety and fuel efficiency of the vehicle. Typically, stamped components are formed at room temperature and include the use of water- and oil-based lubricants to improve formability and reduce the coefficient of friction between the stamping blank and the die surface. Oil- and water-based lubricants have a maximum range between 120°C–250°C. Recent developments in metal forming include elevated temperature operations at 900°C. Lubricants are often used for hot-stamping applications but are not compatible with downstream painting operation and must be chemically removed prior to use in the body shop. Enabling technologies are needed that reduce the friction between the blank and the die surface, allowing uniform metal forming with easy removal of the coating thereby reducing the cost of high-volume manufacturing and improving the overall yield. Previous studies showed that the friction between bare metal surfaces during metal forming is 0.4. Results indicate that it is not feasible to produce a totally acceptable part at such high levels of friction.

Towards this end, 2D nano materials-based lubricants, particularly solution-processed graphene-based solid lubricants developed originally at Argonne National Laboratory, are promising. Based on our previous understanding of performance of 2D-solid lubricants, three novel compositions were developed for warm (temp range 275°C–480°C) and hot stamping (i.e., the blank temperature of 930°C) applications. A first step towards evaluating the solid lubricants was testing the performance in pin-on-disc (PoD) tests (Figure 1). PoD tests showed a decrease of 94% and 66% compared to metal on metal contacts. Following PoD, twist compression tests (TCT) were performed for further testing. The TCT method closely mimics the actual test conditions for stamping applications. TCT of these lubricants showed an over 90% drop in friction compared to uncoated and a 65% drop compared to the commercial lubricants for warm forming conditions for prolonged sliding. Recent results (not shown here) at high temperatures showed an over 60% drop in friction as compared to uncoated.

The next steps involve validating the TCT results with mini-stamping operations and additional testing on the manufacturing lines. Scientific understanding in terms of tribolayer formation and coating adherence are underway.

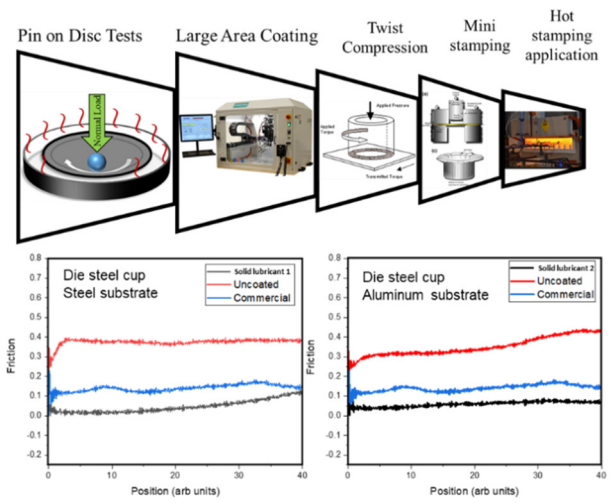

Figure 1. Process flow of the identification of high temperature lubricants. Friction observed with the two solid lubricants showing 65% reduction as compared commercial lubricants for warm stamping applications.

2019 U.S. DRIVE Highlight

Development and Integration of Predictive Models for Manufacturing and Structural Performance of Carbon Fiber Composites in Automotive Applications

ICME technologies for carbon fiber composites for accurate predictability.

General Motors LLC

The goal of this project is to develop an integrated suite of state-of-the-art computational modeling tools based on integrated computational materials engineering (ICME) methodology that are critically needed to enable structural carbon fiber (CF) applications in automobiles. These tools are designed to predict the manufacturing and structural performance of CF composites, including stochastic effects. During the first task of the project, the team calibrated both the manufacturing and structural performance tools, including a stochastic driver, and validated against coupon and component level tests. The targeted difference between predictions and experimental results was limited to less than 15%. During the second task of the project, the manufacturing and performance tools will be integrated by mapping the manufacturing outcomes (e.g., fiber angles, residual stresses, degree of cure, and defects [e.g., voids, dry patches, and wrinkles]) into the structural models. Also, using the tools developed in this project, an automotive assembly currently manufactured in steel is redesigned using CF composites to compare the performance of this assembly with the modeling predictions. Mass savings and cost increase per pound saved compared to the steel assembly will be determined.

In fiscal year (FY) 2019, three large tools were virtually designed to manufacture four large size components of the CF rocker floor assembly that will be used to validate the computational ICME tool development, and assess the lightweighting, manufacturing and structural performance cost metrics compared to the baseline steel assembly. The components of the rocker floor assembly (Figure 1) were manufactured using high-pressure resin transfer molding, a potential game-changing manufacturing technology with 3-5 min. cycle time. The stochastic manufacturing tools developed in the project were validated by comparing the predictions with the experimental data such as pressure, and curing degree measured using multiple sensors embedded in the molding tools. The team observed good correlations. The assembly build task was divided into three phases, and phase-1 build and testing are expected to be completed by the end of FY 2020 Q1.

In FY 2020 Q2, the remaining two phases of the CF automotive rocker assembly build will be completed by incorporating the learnings in the previous phases. The team will validate computational structural performance tools developed in this project by comparing predictions and experimental results for a challenging crashworthiness load case (side pole impact performance) of the assembly. Furthermore, the weight, cost, and performance will be compared with the existing steel design.

The availability to an original equipment manufacturer of integrated computational tools to predict stochastic manufacturing and structural performance of structural composites can potentially enhance enabling technologies and achieve help the substantial lightweighting potentials of CF composites.

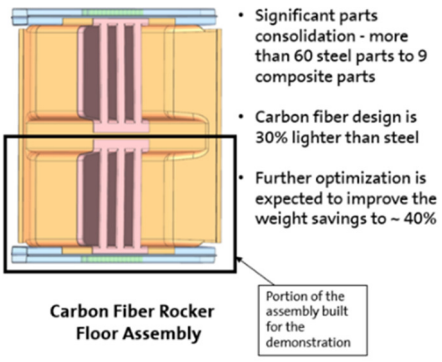

Figure 1. Rocker floor assembly built for demonstration.

2019 U.S. DRIVE Highlight

Thin Advanced High-Strength Steel with Carbon Fiber Reinforced Polymer Coatings

Project developed engineering tools needed for designing a light duty vehicle carbon fiber subframe.

LightMAT Consortium

Recent steel industry advances have led to the development of advanced high-strength steels (AHSS) that can be thinner gauge and thus lighter than conventional sheet steels, while supporting the same vehicle function as thicker gauge conventional steels. Thinner gauge steel panels are subject to inherent sheet forming defects that limit their applicability. Those defects can result in an increased potential for denting, vibration at high vehicle speeds, and "oil canning." The defects are caused by residual stresses induced during coil production and tend to become more exaggerated as the strength level of the rolled sheet is increased to meet the need for thinner, and thus lighter, sheet. Conventional auto body sheet steel averages 1.1 mm thick, ranging from 0.65 mm to 2.5 mm depending on the location. Typical exterior panels are often 0.75 mm thick. Reducing total body panel thickness from 0.75 to 0.55 mm could reduce body mass from 130 to 95 kg (27%). Diversitak has developed a proprietary, low specific gravity, carbon fiber reinforced epoxy (CFRE) that can be applied to AHSS sheet to increase the bending stiffness of the sheet, allowing for thinner gauges of steel to be used compared to what is currently possible. Preliminary testing has proven the concept.

The team applied a thin layer of a CFRE to a stamped sheet of steel with residual stamping oils from the mill, in a time corresponding to automotive processing and processed following automotive e-coat procedures. No problems with adherence or performance were noted. While the CFRE adds weight to a thin gauge steel panel, it is much less weight than is displaced by using thicker conventional mild steel gauges. Steel with the AFRE showed significantly increased dent resistance, oil canning resistance, and part stiffness. Table 1 shows the Flexural Load for different gauges of steel with and without the CFRE coating. A 0.50 mm panel coated with a 0.50 mm CFRE coating can be as stiff as a 0.65 mm uncoated panel.

		Steel Thickness				
		0.50 mm	0.55 mm	0.60 mm	0.65 mm	0.70 mm
CFRE Thickness	0 mm	22 N	29 N	32 N	32 N	35 N
	0.5 mm	36 N	48 N	59 N	N/A	N/A
	1.0 mm	50 N	68 N	79 N	N/A	N/A
	2.0 mm	82 N	104 N	117 N	N/A	N/A

Table 1. Flexural load (N) of DP490 and the CFRE coating applied. CFRE and steel thicknesses were varied.

Environmental corrosion testing was conducted at Idaho National Laboratory, which tested 550 CFRE coated coupons to three separate corrosion test protocols. No corrosion was observed on the CFRE coatings used in either the flexural strength or corrosion evaluation coupon tests after exposure to the tests after 40 cycles. There were no blisters or other corrosion related defects apparent. Additionally, there is no apparent delamination of the coating anywhere on the coupons.

Researchers conducted an extensive cost and mass analysis assuming either full coverage of the door inner or coverage only in predetermined locations. A typical steel door can be downgauged from 0.70 mm thickness to 0.50 mm thickness with the application of a 0.5 mm thick layer of CFRE. If the CFRE is applied for total coverage the mass reduction can be 1.11 Kg per door at a cost of $8.11 per kg ($9.00 per door). If the CFRE is applied to specifically designated areas (patches) then the mass reduction can be 1.55 kg at a cost of $0.12 per kg ($0.19 per door). Even if the patch thickness is increased to 1.0 mm as an additional performance margin, the mass reduction can be 1.54 kg at a cost of $0.23 per kg ($0.35 per door).

2019 U.S. DRIVE Highlight

Machine Learning and Supercomputing to Predict Corrosion/Oxidation of High-Performance Valve Alloys

The first data analytics framework to predict oxidation behavior of automotive high temperature alloys.

Oak Ridge National Laboratory

Strategies for improved fuel efficiency often demand higher operating temperatures for internal combustion engines. However, higher temperatures also significantly accelerate the corrosion/oxidation of key engine components, such as pistons, exhaust valves, and turbo systems. Despite the advanced state of modern computational tools, currently no existing computational approaches can effectively predict the complex high-temperature corrosion and oxidation processes in commercial alloys.

This 3-year project aims to develop practical and highly accurate machine learning models that can rapidly evaluate oxidation of complex, multi-component high-performance valve alloys for turbocharged engines. This project is leveraging Oak Ridge National Laboratory's (ORNL) decades of cyclic oxidation data of high-temperature alloys tested in 10% water vapor at temperatures of 800°C and beyond. These conditions are highly relevant to automotive applications, and have been consistently measured, making the data particularly suitable for modern data analytics.

Figure 1 shows a sample dataset of ORNL's cyclic alloy oxidation data and a trained machine learning model from the first-year effort. While only the simple chemistry of NiCr alloys was used as input features, the results demonstrate that a reasonably accurate model can be trained, although improved accuracy is necessary. This project is also incorporating a range of key scientific features, by calculating and adding high-throughput physics-based simulated data. This will further improve predictive accuracy and allow identification of the underlying mechanism(s) of alloy oxidation. U.S. Department of Energy supercomputers are being extensively used to rapidly populate a large volume of scientific data to augment experimental data, as well as to fill gaps in key fundamental experimental data that is not presently available in the literature.

The team has developed a data analytics frontend toolkit, and has made it publicly available (http://github.com/ornlpmcp/ASCENDS). This versatile software enables machine learning and correlation analysis methods more readily accessible to the broad scientific community.

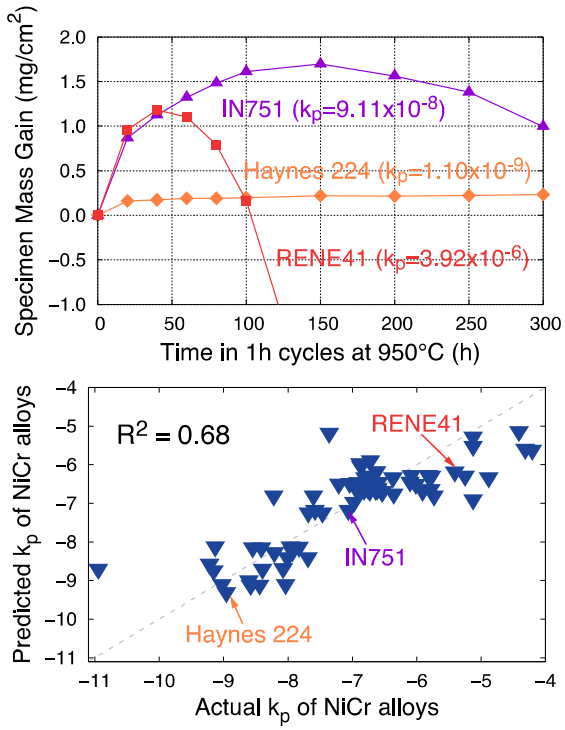

Figure 1. (Top) An example of ORNL s NiCr base alloy cyclic oxidation data at 950 C in air plus 10% water vapor. The lower the parabolic rate constant (k_p), the better oxidation resistance, i.e., Haynes 224 is the best, RENE41 is the worst. (Bottom) A machine learning model trained by correlating composition and oxidation rates of 78 NiCr based alloys from the ORNL dataset. This preliminary model is capable of predicting oxidation behavior of this class of alloys at 950 C in 10% water vapor, and will be further improved by incorporating additional scientific features, for example phase fractions of key precipitates.

2019 U.S. DRIVE Highlight

Higher Conductivity Copper Yields Higher Efficiency Electric Motors

Manufacturing improved copper carbon composites using PNNL developed technology.

Pacific Northwest National Laboratory

During the past decade, the automotive industry has been eagerly seeking materials with the greatest conductivity—or how well a material transports an electric charge—over standard electric copper. The goal is to improve efficiency, weight, power density, and cost of stators and rotors in electric machines like permanent magnet motors, which are recognized for their dependability and higher torque.

To achieve this goal, since 2014 Pacific Northwest National Laboratory (PNNL) researchers have been investigating an alternative to standard copper—ultra-high conductivity copper-graphene composites—creating wire or bar using PNNL's Shear-Assisted Processing and Extrusion technology (ShAPE™).

In copper-carbon composites, carbon additives with high conductivity—for example, graphene—serve as efficient conduits for energy carriers in the composite microstructure. While copper-graphene composites have shown improved conductivity at much smaller scales, methods to fabricate them at industrial scales have been elusive. An effective manufacturing process is critical for distributing the graphene in the copper matrix, synthesizing the composite with minimal porosity, and engineering the copper-graphene interface to minimize carrier scattering, especially at higher temperatures.

Recent advances in PNNL's ShAPE™ technology provide the key to manufacturing at industry scale high-performance copper-carbon composites. ShAPE™ can be used to create extrusions from metals, alloys, and metal composites to manufacture dense, homogeneous microstructures. A billet—or solid block of material—in a stationary container abuts against the flat face of a rotating die. Intense shear and frictional heat plasticizes the billet material at the tool interface, allowing it to flow through the cavity in the tool to form an extrudate.

The team fabricated copper-graphene composite wires measuring 2.5 mm diameter and more than 1 m length *using less than 10 parts per million graphene flakes* (Figure 1). Electrical conductivity of the composites increased as the graphene content increased. Even at such low graphene concentrations, the composites showed 60.8 MS/m or 104.8% IACS electrical conductivity. The composite wires behaved mechanically similar to annealed pure copper samples, owing to the low graphene concentration used in the fabrication process. Processing the copper-graphene composites using ShAPE™ *required only 4% of the ram pressure typically needed* to manufacture standard electric copper wires using conventional extrusion, which point to savings in manufacturing energy as well as streamlined operations.

This constitutes a disruptive approach to light-weighting electric machines such as motors. These composites have several potential applications and can replace conductor-grade copper in electric machines, transmission and distribution cables, transformers, and electronics to enhance conduction efficiency, improved performance, or light-weighting, depending on product need.

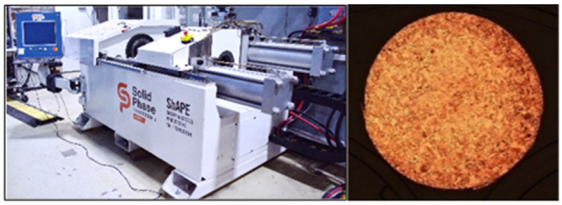

Figure 1. ShAPE™ equipment at PNNL (left) used to make 2.5 mm diameter copper graphene wires with no porosity microstructure (right).

2019 U.S. DRIVE Highlight

Room-Temperature Stamping of High-Strength Aluminum Alloys

Development of processes property modeling techniques to aid in understanding the formability of high strength aluminum alloys.

Pacific Northwest National Laboratory

Automotive components manufactured with aluminum instead of traditional carbon steel could result in a 40%–60% weight reduction, bringing greater vehicle fuel efficiency. The U.S. DRIVE Materials Technical Team Roadmap has identified methods and parameters to improve the formability limits of high-strength aluminum alloys as one of the high priority research needs to help meet the U.S. Department of Energy's targets for 2025: A 25% glider mass reduction relative to a comparable vehicle manufactured in 2015 and at an added cost of no more than $5 per lb. of weight saved.

Pacific Northwest National Laboratory (PNNL) researchers are working to overcome challenges related to stamping or forming high-strength aluminum sheets at room temperature into highly complex, automotive structural components. Although warm/hot-forming practices can eliminate cracking failures during the manufacturing process, such an approach is costly due to more complicated and capital-intensive equipment: heated dies, heat treatments, forming lubricants, and lubricant clean-up. As a result, the use of aluminum sheeting has been limited to lower-strength aluminum alloys and/or manufacture of less-complex shapes such as hoods, deck lids, and inner door frames. In fact, many sheet components are still stamped using steel in the high-volume automotive industry due to such limitations.

To address these challenges, the team is:

- Identifying automotive components that, if formed out of high-strength aluminum, could become lighter-weight versus using high-strength steels.
- Performing stamping simulations to determine if the selected components can be stamped using a high-strength aluminum alloy.
- Integrating microstructure and mechanical performance property models for the selected aluminum alloy.

Based on discussions with original equipment manufacturers and industry partners, the team selected a door side-impact beam currently fabricated in steel (Figure 1) as the prototypical component that, if stamped out of high-strength AA 7075 aluminum alloy, would be beneficial to the automotive industry. Using mechanical property data of the aluminum alloy as input, stamping simulations suggested that fabricating the side-impact beam with the aluminum alloy is feasible. In the third year of this project, sensitive x-ray diffraction experiments were then performed at Brookhaven and Argonne National Laboratories, with the data used to develop initial microstructure and mechanical property models for the AA 7075 aluminum alloy that can qualitatively describe how its strength changes with time after heat treatment. The next step is for the team to stamp a prototype side-impact door beam.

If successful, a lighter-weight and cost-effective side-impact beam would be produced for the automotive industry without sacrificing performance or adding significantly to cost.

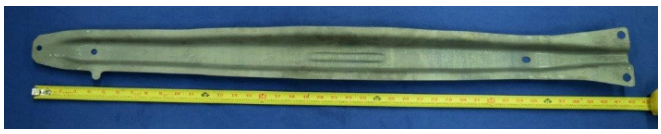

Figure 1. Top view of the steel side impact beam used as a reference to emulate high strength aluminum.

2019 U.S. DRIVE Highlight

Corrosion Control in Carbon Fiber Reinforced Plastic Composite-Aluminum Closure Panel Hem Joints

Development and demonstration of coatings, adhesives, joint geometries, and corrosion test methods to enable vehicle lightweighting via the use of carbon fiber reinforced plastic composites.

PPG Industries

The team of PPG Industries (PPG), Ford Motor Company (Ford), and The Ohio State University (OSU), are developing new coatings and adhesives, new joint geometries, and corrosion characterization techniques to enable the implementation of carbon fiber reinforced polymer inner/aluminum outer (CFRP/Al) lightweight closure panels. The 3-year project involves coating the CFRP with a conductive primer, joining the CFRP to the Al outer with adhesive, producing a hem joint, and then passing the assembled part through the standard automotive paint shop, including electrocoat and topcoat. This approach could result in a weight savings of 40 kg compared to a vehicle with all-Al closure panels and even greater savings compared to steel closures. Rapid implementation of these lightweight materials will require the solutions to fit into the existing automotive manufacturing processes while meeting current specifications for mechanical performance, corrosion resistance, and appearance.

Requirements and challenges for implementation of CFRP/Al hem joints include the following.

- Coatings and adhesives must cure at a lower temperature to enable the use of CFRP.
- Coatings and adhesives must mitigate the mismatch in coefficient of thermal expansion between CFRP and Al.
- Minimize galvanic interactions between CFRP and Al.
- Electrochemical and stress corrosion cracking behavior of the CFRP/Al joint must be tested and understood.
- Development of corrosion tests to predict long-term performance of the joints.

In 2018, the team developed low-cure prototype adhesive and electrocoat formulations that met the cure targets of the project. Electrochemical studies of the CFRP showed variability in the corrosion potential of the CFRP surface that depended on the type of CFRP being studied (twill or chopped fiber). Additionally, accelerated corrosion testing verified increased galvanic corrosion between CFRP/Al.

Based on these results, the project work in 2019 focused on a full-scale prototype demonstration. The team scaled-up the low-cure adhesive and electrocoat formulations and built 5 prototype CFRP/Al liftgates (Figure 1) using standard automotive processes, including adhesive application, pretreatment, electrocoat, and topcoat. The study included low temperature (150°C/10') or standard bakes (175°C/25'). As predicted by finite element modeling, the low-cure adhesive reduced part distortion. The prototype parts were mounted in vehicle position and exposed to various corrosion environments. Teardown of the exposed parts to inspect corrosion is underway. Additional test coupons were prepared and subjected to electrochemical evaluation during a cyclic cabinet corrosion test. Full analysis of corrosion testing will occur in the final year of the project (2020).

Figure 1. Prototype CFRP (black)/Al prototype liftgate.

2019 U.S. DRIVE Highlight

A Multi-Scale Computational Platform for Predictive Modeling of Corrosion in Aluminum-Steel Joints

Project to develop high throughput approaches for the efficient development of materials models to predict various corrosion mechanisms.

University of Michigan

The goal of this project is to develop multi-scale models for predicting the corrosion of aluminum-steel joints used in lightweight vehicle construction. An academia-industry consortium led by the University of Michigan put its expertise to work supported by General Motors with accelerated corrosion tests. The developed models are complete and will be validated by experiments with the goal of achieving strength and fatigue prediction accuracy within 10% of experiments.

This project began January 2019 and will go until December 2021. In this first year, the team selected two joining technologies that are currently used in vehicles, resistance spot welding and self-piercing riveting (SPR) (Figure 1), and a novel new technology, rivet-welding, which is a promising technology for assembling dissimilar metals. The materials are an aluminum alloy, AA 6022, and a hot-dipped galvanized high-strength steel, HDG-HSLA 340. The joints produced by these techniques are susceptible to corrosion, particularly galvanic and crevice corrosion. In the past, tremendous efforts have been devoted to empirical investigation (e.g., salt spray test), and numerical modeling.

The key challenges for efficient yet accurate simulations of corrosion include: (i) phenomenological models with less physics, (ii) less extensible to complex system, (iii) incomplete or less accurate input parameters, and (iv) inaccessible software and database. A multi-scale approach is proposed to develop the computational platform for modeling the corrosion in dissimilar material joints. The innovation of creating a hybrid corrosion initiation and growth model will be transformational, which could combine stochastic corrosion pit initiations and corrosion growth of established pit/crevice or a collection of pits with predetermined anodic and cathode site conditions in one mesoscopic model.

While finite element modeling-based mesoscopic corrosion evolution simulation can be effective in bridging the models in the atomistic and continuum scales, uncertainties involved in the multi-scale modeling as well as the material joint manufacturing processes must be considered. The uncertainty quantification (UQ) must be addressed so that these uncertainty sources and their impacts on the predicted joint performances can be quantified. The research team addresses the UQ challenges by integrating a novel probabilistic confidence-based adaptive sampling technique into the multi-scale simulation platform, which adaptively identifies critical sampling regions with very few multi-scale simulations/experiments for UQ, leading to efficient development of robust homogenized corrosion material models.

Figure 1. The mechanism of corrosion of dissimilar metals due to chemical reactions with the environment such as snow and salt. The reactions are illustrated on a SPR joint (bottom left) and mass loss due to corrosion (bottom right) and its prediction using the models developed by this project.

2019 U.S. DRIVE Highlight

Low-Cost Magnesium Sheet Component Development and Demonstration Project

The USAMP is collaborating on research with academia, materials, coatings and stamping suppliers to accelerate the development of low cost advanced magnesium alloys and sheet forming technology.

United States Automotive Materials Partnership

This project's objective is to research, develop, and demonstrate at least one large, challenging magnesium (Mg) sheet component on a model year 2013 (MY13) or newer vehicle at a manufacturing cost of less than $2.50 per pound of weight saved. To accomplish this, USAMP will research, develop, test, and evaluate at least one Mg alloy and commensurate processing configuration(s) suitable for rolling thin, automotive appearance grade sheet, and forming door inner and outer panels based on the 2013 Ford Fusion as validation.

The three-year project consists of: technical cost guidance to identify key cost drivers associated with current Mg component production; material characterization and modeling studies; rolling trials on ingots; pretreatment, coating application, and lubrication studies; forming studies and scaling to large components; and joining studies. Public data and code developed as part of the project will be curated and hosted in a repository developed and maintained by the LightMAT consortium.

During Year 2, the team completed testing on the baseline alloy ZEK100 and started to evaluate new Mg sheet alloys: E-Form Plus (EFP) commercial sheet, USAMP-derived Alloy 1 (ATMZ3100) and Alloy 2 (ZXME2100). Alloy 1 did not meet formability requirements, so the team focused on Alloy 2. The team determined the final composition of Alloy 2, cast ingots, and rolled thin strips for the USAMP project team's evaluation. Concurrently, a university partner also cast Alloy 2 and processed it with optimized parameters, obtaining better grain texture, surface quality, and elongation.

Forming evaluations performed using the Erichsen deep draw cup test on ZEK100, EFP, and rolled Alloy 2 revealed that EFP is capable of forming the full cup without cracking (Figure 1). Forming the cup at low temperature was a significant barrier, and is a good indication that this project will be able to successfully form door panels. This finding led to a decision to use EFP sheet to form the door panels.

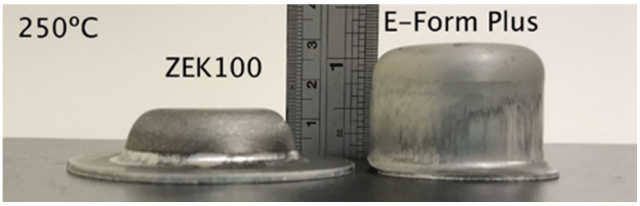

Figure 1. Erichsen cup test of ZEK100 and E Form Plus.

The team performed lubricant and pretreatment evaluations on EFP and compared it to ZEK100. Another project partner developed a process for zinc plating on Mg substrate. Two coating suppliers used tribology testing to identify optimum lubricants which will soon be evaluated via cup testing.

The Joining task scope was revised to focus on EFP using resistance spot welding (RSW), laser welding, and Arplas methods. Initial results show RSW on pretreated EFP can be a viable joining method.

In modeling and validation, the team plans a cross-form stamping test as an intermediate size part to verify simulations. The selected computational simulation code was updated with temperature and strain rate capability to accurately model properties unique to Mg, which is a significant step toward predictive modeling of Mg forming that isn't currently possible.

In summary, while alloy development is a complicated and involved activity, the USAMP's approach is to conduct important assessments of the state-of-the-art and thereby spur improvements in Mg warm forming capability process simulation, as well as in coatings and lubricant technology for warm forming of Mg sheet.

INFRASTRUCTURE AND INTEGRATION

Grid Interaction

2019 U.S. DRIVE Highlight

Unified Model Tying Electric Vehicles with Other Grid Energy Resources Now Available for Researchers

Test data collected and model validation achieved for electric vehicles operating as a grid service.

Argonne National Laboratory

As part of a larger effort to modernize the electric grid, this project defined (modeled) the capabilities of grid-connected devices, so that controls could be developed to enhance the overall grid efficiency, stability, and reliability. Argonne National Laboratory's (ANL) responsibility was modeling and validating electric vehicles (EVs) as a grid resource during charging. ANL ran tests to characterize the physics and control response of three EV models: BMW i3, Nissan Leaf, and Chevy Bolt. The team validated the models by running a realistic multi-day schedule using a combination of charging and driving on a chassis dynamometer. Figure 1 shows a portion of model validation results of a Chevy Bolt EV undergoing a multi-day test including controlled variations in charging rate.

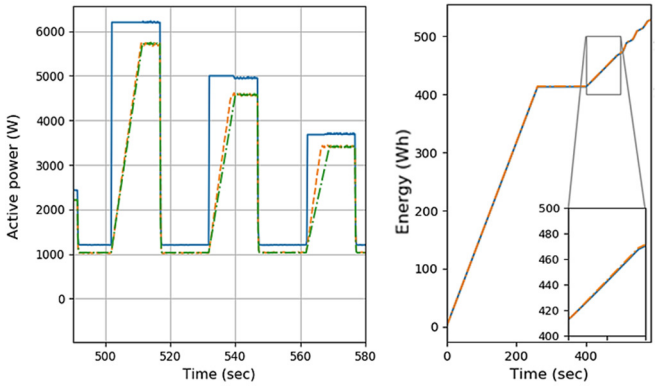

Figure 1. Model validation of Chevy Bolt during transient response testing (left) and tracking energy throughout realistic charging schedule (right).

Subsequently, ANL modeled the behavior of individual drivers (agents) as they carried out their own unique activity schedules, including while driving, parked, and parked while charge-connected, using data from car manufacturers and the U.S. Department of Transportation's National Household Transportation Survey. The agent-based method provides the foundation to model the aggregate EV fleet response with various types of grid service requests (requests to raise or lower charging power depending upon real-time grid needs). Pre-planning charge times showed a high degree of flexibility for the grid operator, who can request reduction in load by either reducing charge rates or even turning off some vehicle chargers, and vice versa. Figure 2 shows example results illustrating how changes in the makeup of charging strategies can have favorable impacts on the peak power demand of the entire fleet of vehicles.

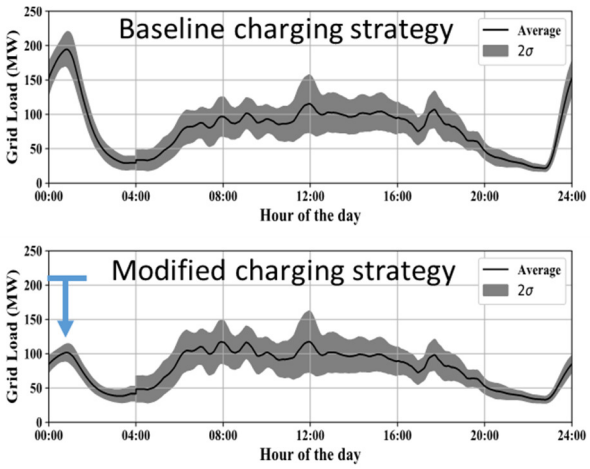

Figure 2. Aggregate grid load results from agent based model representing 200,000 vehicles with two different charging strategies.

Other DOE National Laboratories provided models for electric water heaters, solar panels, and commercial refrigeration units, among others. With this computer code, researchers can now find new ways to improve grid efficiency and reliability by experimenting with different controls for grid-connected devices. The code is open source and leverages modern modular writing methods so that new devices can be easily added. The code is free and available for researchers on GitHub and the GMLC Open Library websites.

2019 U.S. DRIVE Highlight

Electric Vehicle Market Projections: Scenarios and Impacts

Electric vehicle adoption tool projects the composition of the light duty vehicle fleet through 2050, providing utilities a resource for understanding the impact of electric vehicles on service territories.

Electric Power Research Institute

Although the light-duty plug-in electric vehicle (EV) industry has steadily expanded over the past 10 years, the EV market is still in the early stages of expansion. Utilities have initiated programs to prepare for a significant market penetration of EVs within their service territories. In order to provide the best service and reliability for their customers, utilities need to know the expected number of EVs in their service areas and the impacts of the EVs on their systems. To help utilities and other parties to adequately prepare for the market penetration of EVs, the Electric Power Research Institute (EPRI) maintains an EV market adoption tool that estimates and projects the composition of the on-road vehicle fleet through the year 2050 (Figure 1). The tool calculates EV energy use, greenhouse gas emissions reduction, and the high-level impacts of shifting vehicle energy consumption from liquid fuel to electricity.

In 2019, the project team updated the adoption tool to reflect new data on actual EV sales and market conditions. The team analyzed the latest EV registration data and market intelligence to develop EV sales estimates for each light-duty vehicle model annually over the period from 2019 through 2022. To create market adoption scenarios for the longer term, the team analyzed available EV forecasts, reports, and incentive programs from several external government and commercial sources. Based on these data, three national-level scenarios were selected to represent a plausible range of outcomes. EPRI's EV projection algorithms then tailor the three scenarios to the county level based on recent local EV registration data and regional constraints for California and other states that comply with the California zero-emissions vehicle (ZEV) regulation.

The EV adoption tool generates spreadsheets that illustrate the projected market growth and broad-based impacts of EVs within any specific utility service territory or other region within the contiguous United States. The software calculates the market penetration of different vehicle classes (i.e., categories of vehicles based on typical usage patterns) and powertrain types (i.e., conventional vehicles and various types of EVs). A vehicle turnover model uses aging data and survival estimates to simulate the evolution of the vehicle fleet over time. The tool draws on a variety of external data sources to inform its calculation of vehicle energy use and greenhouse gas emissions. The results are presented for each of the three default scenarios, which are valuable to illustrate possible future trajectories of the vehicle fleet and associated utility impacts.

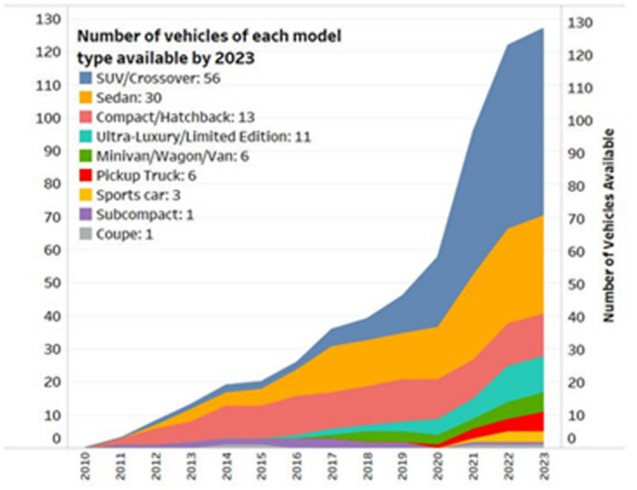

Figure 1. EV market outlook through 2023.

The Energy Management Circuit Breaker, Phase 2

Field testing of a circuit breaker that embeds metering, control, electric vehicle charging, and communications.

Electric Power Research Institute

The Electric Power Research Institute (EPRI) is working with a group of nine utilities to field and demonstrate a standard format electrical circuit breaker that embeds communications, metering, and control functionality. Two versions of the device, referred to as the Energy Management Circuit Breaker (EMCB), are being deployed (Figure 1):

- A standard version that offers on/off control; and
- An electric vehicle version that embeds an SAE J1772 charging interface in the breaker (Figure 1).

Why embed intelligence and metering in circuit breaker?

- The service panel is the heart of a facility's electrical system;
- All end use loads are on a breaker;
- Major loads are on dedicated breakers;
- Miniaturization of communications and metrology hardware is an enabler;
- Many potential use cases and applications; and
- Potential lower cost solution or end use monitoring and control.

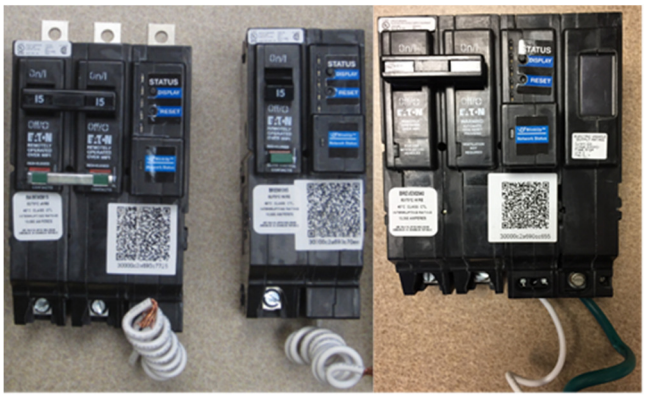

Figure 1. The EMCB single and double pole standard versions (left); electric vehicle version (right).

Devices are currently being fielded with software tools, the key focus of the development work. A nominal 250 devices will be deployed by the first quarter of 2020 (see Figure 2).

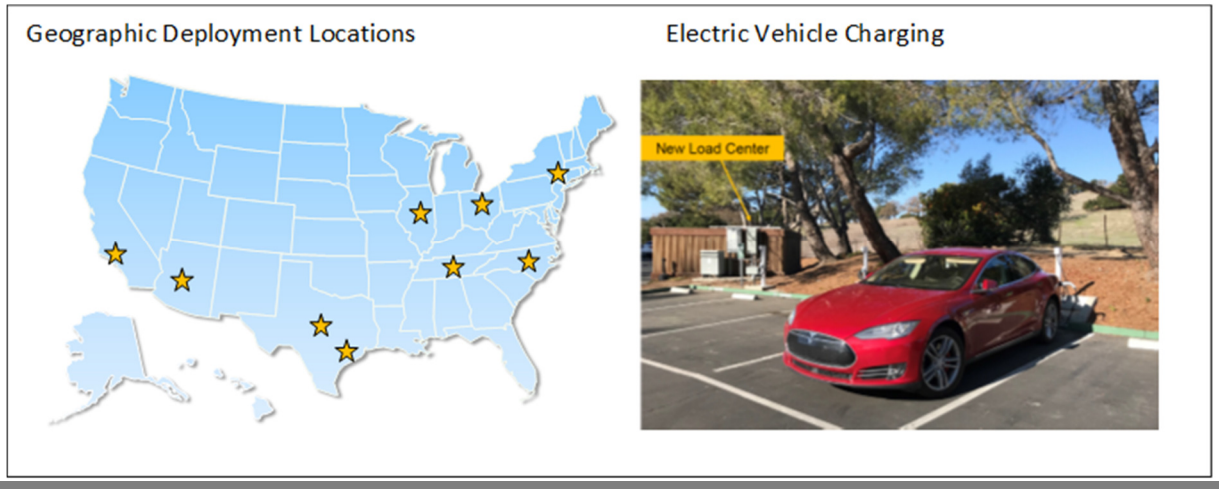

Figure 2. (Left) Geographic location of the deployment. (Right) Sample EMCB deployment.

Hydrogen Codes and Standards

2019 U.S. DRIVE Highlight

Development of an In-Line Hydrogen Contaminant Detector

Development of a low cost in line hydrogen contaminant detector capable of detecting SAE J2719 levels of critical impurities in hydrogen fuel.

Los Alamos National Laboratory

Los Alamos National Laboratory (LANL) has developed and patented (U.S patent 10,490,833) a hydrogen contaminant detector (HCD) capable of measuring impurities in a dry hydrogen fuel stream. This detector is based on a hydrogen pumping cell using a Nafion® membrane and a water wicking system, which ensures stable proton conductivity. The HCD is capable of detecting the presence of high impact contaminants in excess of the limits set by the SAE J2719 fuel quality standard. Currently, hydrogen refueling station (HRS) operators assess fuel quality by performing expensive laboratory analysis semi-annually or when major equipment is replaced that can affect fuel quality. Between these infrequent analyses, fuel quality deviations beyond limits could result in unacceptable contamination of fuel cell vehicles. Therefore, HRS operators currently are exploring conventional gas analyzers, like non-dispersive infrared (NDIR) analyzers for carbon monoxide detection, to supplement their fuel quality efforts. However, these analyzers are expensive, need climate-controlled enclosures, require frequent calibration, are prone to drift, and are specific to only single contaminants.

The LANL HCD utilizes an ultra-low loaded, sputtered platinum (Pt) (≈ 0.04 mgPt/cm^2) working electrode that is very sensitive to any impurities in the hydrogen stream. Because this electrode is similar to the one used in a fuel cell, any contaminant that affects the fuel cell electrode will result in a significant decrease in hydrogen pumping current of the HCD. Figure 1 illustrates the percentage loss in pumping current observed when the HCD is exposed to various CO concentrations injected into the hydrogen stream. The pumping current loss (%) increases in proportion to the logarithm of the CO concentration in the hydrogen, thereby exhibiting excellent sensitivity at low CO concentrations.

The LANL HCD has been field tested at the H2Frontier fueling station in Burbank, California and has proved superior to the existing NDIR system in baseline drift, sensitivity, and accuracy to CO. This HCD, similar to any analytical instrument like the NDIR, needs to be operated on a slip stream of main hydrogen fueling flow. Moreover, the water supply to the wicking system needs to be refilled regularly and the potentiostat used to measure the pumping current is expensive. LANL is currently working with Skyre, Inc. on a technology commercialization fund effort to develop low-cost electronics and to commercialize this important technology. LANL is also working to eliminate the humidification system by developing membranes that can maintain their proton conductivity under dry conditions.

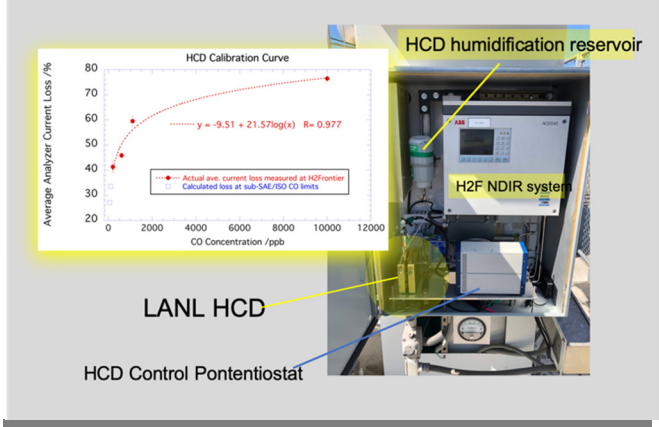

Figure 1. LANL HCD installed at the H2Frontier HRS and its response to various concentrations of CO.

Hydrogen Delivery

2019 U.S. DRIVE Highlight

Hydrogen Refueling Station Footprint Analysis

Identification and quantification of opportunities to reduce fueling station footprint.

Sandia National Laboratories and the National Renewable Energy Laboratory

A team led by Sandia National Laboratories has completed rigorous analysis of the impact of fueling station designs on land area requirements (i.e., "footprint"), and opportunities to reduce station footprint using recent code revisions and new station technologies. Footprint is a key barrier to the deployment of fueling stations, especially in dense urban areas where hydrogen demand is high but space for fueling stations is limited. A significant focus of this study was the setback distances prescribed by the National Fire Protection Association (NFPA)-2 Hydrogen Technologies Code, between potential points of hydrogen release and other aspects of a fueling station (e.g., equipment, air intakes, parked cars, or buildings).

The team analyzed generic station designs (Fig.1) that each had a capacity of 600 kg/day and 4 dispensers. The three base case designs differed in their method of hydrogen supply, including use of gaseous hydrogen tube trailers, liquid hydrogen tankers, and on-site electrolysis production. These station designs were then iterated on to study the impacts of recent changes to NFPA-2, colocation with gasoline refueling infrastructure, innovative delivery technologies, underground storage of hydrogen, and rooftop storage of hydrogen, all of which resulted in a total of 32 different station designs. The footprint of the base case stations ranges from 13,221 to 21,250 ft².

While the prescribed setback distances in NFPA-2 can be significant, it was found that these setback distances had a nuanced impact on overall station size. For example, the driveway required for hydrogen delivery trucks was found in many cases to be the dominant driver of overall lot size. Key conclusions of the report regarding methods to reduce footprint included: 1) Using innovative hydrogen delivery tube trailers or tankers with shorter turn radii, or eliminating their use altogether (e.g., through onsite production) can reduce station footprint by up to 18%. 2) Using new setback distances in the 2020 edition of the NFPA-2 code, which treat gaseous and liquid hydrogen handling technologies differently at liquid fueling stations, can reduce station footprint by up to 14%. 3) Using underground storage systems or vaults can reduce station footprint by up to 27%.

The team estimated the cost of underground burial of hydrogen storage tanks, and the "break-even" cost of land at which underground burial is cost-competitive; and provided a case study of how "alternative means" can be utilized to design a station that has smaller setback distances than the prescriptive setback distances within NFPA-2. "Alternative means" refers to guidelines that can be used within NFPA-2 to enable the implementation of shorter setback distances, provided that the station design still meets the intent of the code's prescriptive requirements.

The station designs from this analysis can be used to inform stakeholders within hydrogen infrastructure on opportunities within the code and in the area of technology R&D to reduce station footprint, and thereby enable cost-competitive station deployment in more regions of the U.S. than otherwise feasible.

Figure 1. Example real world hydrogen fueling station layout.

Hydrogen Production

2019 U.S. DRIVE Highlight

New PGM-Free Catalysts and Membranes Improve Performance of Alkaline Membrane Electrolyzers

Research projects make improvements in membrane performance and durability and replace expensive components to reduce capital cost.

Northeastern University and Los Alamos National Laboratory

Alkaline exchange membrane (AEM) electrolysis has the potential to be a less costly alternative to proton exchange membrane (PEM) electrolysis. Using an AEM (differing from conventional commercial alkaline electrolysis systems) enables incorporation of a wider range of stable, low-cost materials and components, including platinum group metal (PGM)-free catalysts. However, AEM electrolysis is at a much earlier development stage than PEM electrolysis. Two AEM electrolysis projects have made great strides towards increasing the performance and durability of membranes and catalysts, and decreasing capital costs. This research is essential to achieve the U.S. Department of Energy's (DOE) $2/kg-hydrogen ($H_2$) cost goal for H_2 production.

Los Alamos National Laboratory (LANL), led by Yu Seung Kim, has successfully prepared poly(styrene-b-ethylene-b-styrene) AEMs that meet conductivity, stability, and mechanical property targets with a 78% decrease in reagent cost compared to competitive aromatic membranes. These novel membranes exhibit excellent stability as they show no decrease in conductivity after 300 h of testing in 1 M sodium hydroxide at 80°C. Also, these membranes are easy to synthesize, scalable, and comprise a more environmentally benign synthetic route than current membranes.

In addition to these performance and cost improvements, LANL has investigated AEM electrolyzer durability-limiting factors. This effort has identified the critical degradation mechanism of the membrane as phenyl electro-oxidation. Understanding the nature of this detrimental process is useful in designing new, more durable components for AEM electrolysis.

Work at Northeastern University, orchestrated by Sanjeev Mukerjee, is helping to eliminate expensive and rare metals from the electrolyzer. These costly PGMs are commonly used in electrolyzers for their ability to catalyze the hydrogen evolution (HER) and oxygen evolution (OER) reactions without losing activity over time. These materials are prohibitively expensive, creating a barrier to meeting DOE's H_2 production cost targets. PGM-free nickel-based catalysts have demonstrated a potential reduction of ~50 mV compared to state-of-the-art iridium oxide for the OER at 500 mA/cm² (Figure 1). Also, through a combination of new materials development and membrane electrode assembly (MEA) optimization over the last 2 years, the researchers have developed fully PGM-free MEAs with a ~300 mV improvement in performance at 500 mA/cm².

These advancements are extremely encouraging, highlighting the potential benefits of low-cost AEM electrolyzers. However, achieving the $2/kg-$H_2$ production cost goal will require further technological advancements, including improved performance, durability, and efficiency and decreased capital costs.

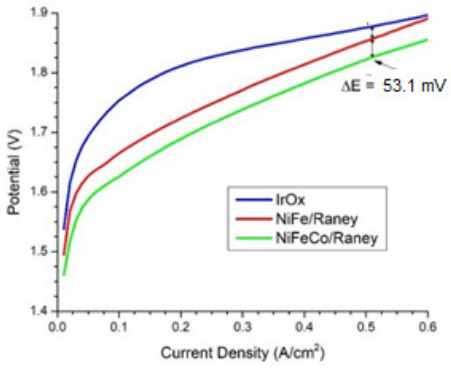

Figure 1. Comparison of AEM polarization curves: PGM free (red and green) with PGM (blue) OER catalysts. Pt/C used as HER catalyst for all. Cell operated at 50 C with 1% K_2CO_3.

2019 U.S. DRIVE Highlight

Path to $2/kg Hydrogen from Polymer Electrolyte Membrane Electrolysis Identified

New analysis highlights the potential for centralized and distributed hydrogen production from highly efficient polymer electrolyte membrane electrolysis.

Strategic Analysis, Inc.

Researchers performed rigorous technoeconomic analysis on state-of-the-art polymer electrolyte membrane (PEM) electrolyzers quantifying key cost drivers and identifying potential pathways to reach the U.S. Department of Energy's (DOE) hydrogen (H_2) production cost goal of less than $2/kg (Table 1). Achieving this goal will require further advancements in the technology, including improved durability and efficiency and decreased capital costs. It also depends significantly on realizing low electricity costs consistent with the H2@Scale vision.

The global H_2 market is at present largely supplied from natural gas-derived H_2. However, PEM electrolysis shows promise as an economical, clean and sustainable option for large-scale H_2 production, using only water and electricity which can come from renewables, as inputs.

PEM H_2 production costs were found to range from ~$2.10 to $7.04/kg in this study. Strategic Analysis, Inc. and the National Renewable Energy Laboratory prepared case studies of the cost of PEM H_2 production using the recently revised Hydrogen Production Analysis Model (H2A) Version 3.2018.[4] These case studies are an update to the previous analysis conducted in 2014 and are now available as a reference case study (Table 1.)[5] Four case studies were conducted; two Distributed Production (1,500 kg H_2/day), and two Central Production (50,000 kg H_2/day) for both projected current (2019) and projected future (2035) technology years. All cases assume a high-volume manufacturing rate of 700MW/year for each case.

PEM technology has shown significant advancements, including improvements in performance and durability achieved with DOE support. To ensure the relevance and accuracy of the study parameters and results, researchers solicited information from four independent manufacturers of PEM electrolysis systems. Reported data includes: engineering system definition; capital costs; operating costs; variable and fixed expenses; and replacement costs. The results of these new case studies will guide research and development efforts to further the goals of low-cost and sustainable H_2 production.

Electricity price remains a primary cost driver in all cases, which emphasizes the importance of increasing electrical efficiency and also leveraging low-cost electricity when available. The baseline cases in Table 1 assume an averaged electricity pricing of ~$0.07/kWh, while the special assessments based on electricity pricing of $0.03/kWh highlight how the DOE cost goal could be met in low-cost electricity scenarios.[6]

Case Study	Low Value	Baseline Value	High Value	3¢/kWh Electric
Distributed Production				
Current	$2.82	**$4.99**	$7.04	$2.54
Future	$2.10	**$4.48**	$6.04	$1.92
Central Production				
Current	$2.53	**$4.83**	$6.89	$2.31
Future	$2.07	**$4.48**	$6.05	$1.86

Table 1. High volume cost projections for PEM electrolysis H_2 production. Low and high values reflect expected cost spread (90% certainty, Monte Carlo analysis). ($/kg$H_2$).

[4] See https://www.hydrogen.energy.gov/h2a_production.html.
[5] See https://www.hydrogen.energy.gov/pdfs/14004_h2_production_cost_pem_electrolysis.pdf.
[6] Electricity prices from Energy Information Administration (EIA) Annual Energy Outlook (AEO) 2017 Report.

Integrated Systems Analysis

2019 U.S. DRIVE Highlight

Past Growth in U.S. Electric Load Exceeds Additional Consumption and Peak Demand in Future EV Scenarios

Comparing future EV scenarios and historical trends offers insights for impacts on bulk power systems.

Grid Interaction Technical Team and Integrated Systems Analysis Technical Team

Electric vehicles (EVs) can meet U.S. personal transportation needs by using domestic energy resources while also offering carbon and pollutant emissions benefits. However, wide-scale adoption of light-duty EVs will require assessment of and possible modification to U.S. electric power generation and distribution systems. The Grid Interaction and the Integrated Systems Analysis Technical Teams collaborated to examine a range of future EV market penetration scenarios (low, medium, and high) and associated changes to the bulk U.S. electric power system in terms of energy generation and generation capacity compared to historical trends in both. The comparisons illustrate that there have been sustained periods where growth in load exceeded the ranges of additional electricity consumption and peak demand associated with the future EV market scenarios considered here.

The latter half of the 20th century included periods of annual electricity generation growth equivalent to the energy consumption of as many as 25 million new light-duty EVs (equivalent to roughly 150% of all new light-duty vehicle sales in the United States today). Periods of highest growth in electricity generation (in the 1970s and 1990s) included expansions to baseload generation from nuclear and fossil resources at a time when the policy environment allowed for necessary investment. In contrast, over the last 10 years, stagnant electricity demand has moderated growth in electricity generation to near zero, with new generation capacity mostly being deployed to offset the retirement of legacy power plants. Significant growth in the EV market could change that trend.

Despite this flat trend in electricity demand over the last decade, the U.S. electric power system added an average dispatchable generating capacity of 12 GW per year, with years that exceeded 25 GW when intermittent resources are included (Figure 1). In an uncoordinated charging scenario (chosen as an illustrative worst case), 12 GW of dispatchable generating capacity is equivalent to the aggregate demand of nearly 6 million new EVs. This number does not account for managed charging (i.e., using smart communications technology to coordinate EV charging), which offers additional flexibility to reduce peak demand and align load with supply availability, both of which will play an important role in facilitating integration of EVs at scale.

Also, non-technical factors (such as policy, regulatory framework, and economic constraints) may have changed over the historical periods considered and may affect future electricity generation and expansion of generation capacity. Additionally, potential challenges—such as distribution system expansion (e.g., for high-power charging or due to legacy infrastructure constraints), transmission constraints, operation constraints (such as ramping capabilities and spinning reserve requirements), and medium- and heavy-duty vehicle charging—warrant further study. Other more detailed U.S. DOE efforts already underway intend to study such potential impacts.

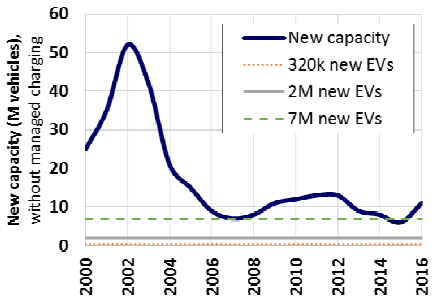

Figure 1. Dispatchable (non renewable) grid capacity installations over time versus equivalent need for 320k, 2M, and 7M new EVs market scenarios.

2019 U.S. DRIVE Highlight

Automated Vehicle Lightweighting and Smooth Driving Offset Automation Load for a Net Reduction in Greenhouse Gas Emissions in Base Case 2030 Scenario

An environmental analysis of automated vehicles with various levels of automation loads.

Integrated Systems Analysis Technical Team

Introduction of connected automated vehicles (CAVs) is likely to transform mobility with profound societal and environmental ramifications. The Integrated Systems Analysis Technical Team (ISATT) of the U.S. DRIVE partnership evaluated the cradle-to-grave (C2G) greenhouse gas (GHG) emissions of conventional and CAV technologies for a midsize sport utility vehicle (SUV) in 2030. Powertrains considered were internal combustion engine vehicle (ICEV), hybrid electric vehicle (HEV), battery electric vehicle (BEV), and fuel cell electric vehicle (FCEV).

The ISATT expanded Argonne National Laboratory's Greenhouse gas, Regulated Emissions, and Energy use in Transportation (GREET®) model to conduct the C2G GHG emissions analysis of CAVs. The net per-mile GHG emissions of CAVs is complicated by the large number of factors that need to be considered, such as the burdens associated with production and use of automation sensors and computing hardware, as well as the benefits of mass reduction, smooth driving (reduced rapid acceleration and deceleration), decreased need for vehicle safety equipment, and induced travel demand. The study considered three possible automation power loads: 200 W, 1,000 W, and 2,000 W; a 20% vehicle weight reduction; and an increase in CAV lifetime vehicle miles traveled (VMT) to 500K (compared to a 200K baseline)[7]. The C2G analysis included GHG emissions for both fuel and vehicle cycles. The fuel cycle includes fuel production emissions and emissions associated with fuel consumption during use. The vehicle cycle includes acquisition of vehicle materials, vehicle manufacturing, and end-of-life disposal and recycling of vehicle components.

Figure 1 illustrates C2G GHG emissions for the baseline conventional SUV (1) and impacts of base case assumptions of 20% decreased mass (2), increased VMT to 500K (3), 1000-W automation power load (4), 15% fuel economy benefit from drive smoothing (5), and C2G emissions for the base case CAV (6). The GHG reduction associated with mass reduction and smooth driving more than offset the increased GHG emissions due to CAV loads.

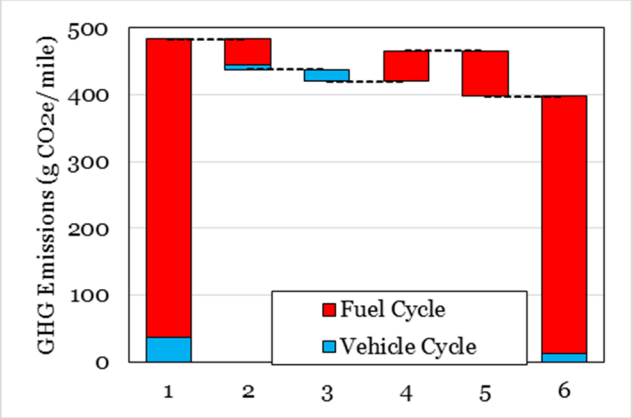

Figure 1. C2G GHG emissions of the conventional baseline SUV (1) and impacts of base case assumptions for mass reduction (2), increased VMT (3), CAV power demand (4), and drive smoothing (5), resulting in emissions for the base case CAV (6).

Table 1 shows baseline C2G GHG emissions (gCO_{2e}/mile) for different conventional powertrains, changes with automation, and final results for CAVs.

	ICEV	HEV	BEV	FCEV
Baseline (non-AV)	485	317	287	312
Reduced Mass	-45	-36	-21	-26
Increased VMT	-18	-19	-38	-29
Automation	45	36	16	23
Smooth Driving	-68	-43	-33	-39
CAV	399	256	211	240

Table 1. Automation effects on SUVs with different powertrains.

[7]See https://www.nrel.gov/docs/fy17osti/67216.pdf.

(This Page Left Intentionally Blank)